On Accurately Estimating Stability Thresholds for Periodic Spot Patterns of Reaction-Diffusion Systems in $\mathbb{R}^2$

D. IRON, J. RUMSEY, M. J. WARD, and J. WEI

David Iron; Department of Mathematics, Dalhousie University, Halifax, Nova Scotia, B3H 3J5, Canada,
John Rumsey; Faculty of Management, Dalhousie University, Halifax, Nova Scotia, B3H 3J5, Canada,
Michael Ward, Juncheng Wei; Department of Mathematics, Univ. of British Columbia, Vancouver, B.C., V6T 1Z2, Canada.

In the limit of an asymptotically large diffusivity ratio of order $\mathcal{O}(\varepsilon^{-2}) \gg 1$, steady-state spatially periodic patterns of localized spots, where the spots are centred at lattice points of a Bravais lattice, are well-known to exist for certain two-component reaction-diffusion systems (RD) in $\mathbb{R}^2$. For the Schnakenberg RD model, such a localized periodic spot pattern is linearly unstable when the diffusivity ratio exceeds a certain critical threshold. However, since this critical threshold has an infinite order logarithmic series in powers of the logarithmic gauge $\nu \equiv -1/\log \varepsilon$, a low-order truncation of this series is expected to be in rather poor agreement with the true stability threshold unless ε is very small. To overcome this difficulty, a hybrid asymptotic-numerical method is formulated and implemented that has the effect of summing this infinite order logarithmic expansion for the stability threshold. The numerical implementation of this hybrid method relies critically on obtaining a rapidly converging infinite series representation of the regular part of the Bloch Green's function for the reduced-wave operator. Numerical results from the hybrid method for the stability threshold associated with a periodic spot pattern on a regular hexagonal lattice are compared with the two-term asymptotic results of [**10**] [Iron et al., J. Nonlinear Science, 2014]. As expected, the difference between the two-term and hybrid results is rather large when ε is only moderately small. A related hybrid method is devised for accurately approximating the stability threshold associated with a periodic pattern of localized spots for the Gray-Scott RD system in $\mathbb{R}^2$.

Key words: singular perturbations, localized spots, summing logarithmic expansions, Bravais lattice, Floquet-Bloch theory, Green's function.

1 Introduction

Spatially localized spot patterns occur for various classes of reaction-diffusion (RD) systems with diverse applications to theoretical chemistry, biological morphogenesis, and applied physics (cf. [**27**], [**28**], [**20**]). More generally, a wide range of topics in the analysis of far-from-equilibrium patterns modeled by PDE systems are discussed in [**22**].

In this paper we formulate and implement a hybrid asymptotic-numerical theory for accurately calculating a stability threshold for a periodic pattern of localized spots in $\mathbb{R}^2$ that occur for two specific singularly perturbed RD systems of the general form

$$(1.1) \qquad v_t = \varepsilon^2 \Delta v + f(u,v), \qquad \tau u_t = D \Delta u + g(u,v).$$

Here $0 < \varepsilon \ll 1$, $D > 0$, and $\tau > 0$ are parameters. The two specific systems we consider are a simplified form of the Schnakenberg model, for which $f(u,v) = -v + uv^2$ and $g(u,v) = a - \varepsilon^{-2}uv^2$ where $a > 0$, and the Gray-Scott (GS) model, for which $f(u,v) = -v + Auv^2$ and $g(u,v) = (1-u) - uv^2$ where $A > 0$. Our analysis for each of these systems will focus on the semi-strong interaction regime characterized by $\varepsilon \to 0$ with $D \geq \mathcal{O}(1)$. In the limit $\varepsilon \to 0$, each of these two systems support localized steady-state spot patterns, where the localized spots for v are taken to be centred at the lattice points of a general Bravais lattice Λ.

There is a rather extensive literature on the existence and stability of 1-D spike patterns on the finite and infinite

line for specific two-component RD systems, such as the Gierer-Meinhardt (GM) and GS models, in the semi-strong regime (cf. [**6**], [**7**], [**26**], [**9**], [**31**]). On a bounded 2-D domain with Neumann boundary conditions, a leading order in $\nu \equiv -1/\log \varepsilon$ rigorous theory was developed to analyze the stability of multi-spot steady-state patterns for the GM model (cf. [**32**], [**33**]), the Schnakenberg model (cf. [**35**]), and the GS model (cf. [**34**]), in the parameter regime where $D = D_0/\nu \gg 1$ in (1.1). One of the key results of [**35**] for the stability of multi-spot patterns on a finite domain for the Schnakenberg model is that there is a stability threshold, corresponding to a zero eigenvalue crossing, that occurs when $D = \mathcal{O}(\nu^{-1})$ where $\nu \equiv -1/\log \varepsilon$, with the pattern being linearly stable only when D is below this threshold. This instability is manifested as an asynchronous, or sign-fluctuating, perturbation in the amplitudes of the localized spots, and it triggers a nonlinear mechanism leading to the annihilation of only some of the spots in the pattern. As such, this instability has been termed a competition instability (see [**33**], [**34**], and [**5**] for an analysis of this instability for several RD systems). Other instabilities, such as spot self-replication processes, can occur for certain RD systems of the form (1.1) when $D = \mathcal{O}(1)$. In particular, a hybrid asymptotic-numerical theory to analyze spot self-replication instabilities on a bounded 2-D domain for the Schnakenberg and GS models was given in [**11**] and [**5**], respectively. A similar analysis for the Brusselator model on the surface of a sphere was given in [**25**].

In [**10**] the linear stability of a periodic pattern of spots for the Schnakenberg model was investigated. For $\varepsilon \to 0$, the method of matched asymptotic expansions was used to construct a steady-state localized one-spot solution within the fundamental Wigner-Seitz cell of the lattice, and this solution was then extended periodically to all of $\mathbb{R}^2$. To determine the linear stability of this solution with respect to $\mathcal{O}(1)$ time-scale instabilities arising from zero eigenvalue crossings, the Floquet-Bloch theorem was used in [**10**] to formulate a singularly perturbed eigenvalue problem in the Wigner-Seitz cell Ω with quasi-periodic boundary conditions on $\partial\Omega$. From an analysis of this eigenvalue problem, it was shown that there is a continuous band of real spectra lying close to the origin in the spectral plane, which satisfies $|\lambda| = \mathcal{O}(\nu)$ where $\nu \equiv -1/\log \varepsilon$, when the inhibitor diffusivity D satisfies $D = D_0/\nu + \mathcal{O}(1)$ for some leading-order stability threshold D_0. However, since D_0 is independent of the lattice geometry, and depends only on the area $|\Omega|$ of the Wigner-Seitz cell and the parameter $a > 0$ in the Schnakenberg model, the effect of the particular lattice arrangement of spots on the stability threshold only occurs at a higher order term in the expansion of the stability threshold for D. Upon fixing $|\Omega| = 1$, in [**10**] a two-term expansion for the stability threshold in the form $D = D_0/\nu + D_1 + o(1)$ was calculated, where D_1 was found to depend on the lattice arrangement of spots through the regular part of the Bloch Green's function for the Laplacian. By optimizing D_1, it was shown in [**10**] that a regular hexagonal arrangement of localized spots has the largest diffusivity threshold. This result of [**10**] is given below in (3.22) of §3. In §2 we give a very brief outline of lattices and reciprocal lattices, while in §2.1, we introduce the Bloch Green's function and derive a key property for its regular part.

More generally, the competition stability threshold for a periodic pattern of spots for the Schnakenberg model has an infinite logarithmic series in powers of $\nu = -1/\log \varepsilon$ of the form $D = \nu^{-1}\mathcal{D}(\nu)$, where $\mathcal{D}(\nu)$ is an infinite series in powers of ν, with $\mathcal{D}(0) = D_0$ and $\mathcal{D}'(0) = D_1$. Since the logarithmic gauge ν decreases very slowly as ε decreases, many terms in this series are typically needed to provide an accurate quantitative prediction of the stability threshold when ε is only moderately small. In 2-D dimensional domains, related infinite logarithmic expansions also arise in the analysis of singularly perturbed eigenvalue problems (cf. [**30**], [**12**]), in calculating the mean first passage time for a Brownian particle to leave a domain through a narrow gap (cf. [**24**]), in nonlinear biharmonic problems of MEMS (cf. [**16**]), and in determining the drag coefficient for slow viscous flow past a cylinder (cf. [**14**], [**8**]). A unified theoretical framework to treat such diverse problems with infinite logarithmic series is surveyed in [**29**].

One main goal of this paper is to formulate a hybrid asymptotic-numerical method to calculate an approximation for the competition instability threshold for the Schnakenberg model that is accurate to all orders in ν. Instead of determining the individual terms in the infinite series representation of $\mathcal{D}(\nu)$, in §3 we derive a new reduced problem that, when solved numerically, has the effect of summing the infinite series for this stability threshold. This reduced problem, in the form of the scalar nonlinear algebraic equation given in (3.19) below, involves both a nonlinear function associated with the steady-state construction of the locally radially symmetric spot profile as well as the regular part of the Bloch Green's function for the Laplacian. Results for the optimal stability threshold from our new hybrid method is compared with the two-term asymptotic result of [**10**].

The second main goal of this paper is to extend the hybrid theory to accurately determine the competition stability threshold for a periodic pattern of spots for the GS model. For a fixed D, ε, and lattice arrangement of spots, in §4 we formulate a new reduced problem that determines the competition stability threshold value of the feed-rate parameter A that is accurate to all orders in $\nu \equiv -1/\log \varepsilon$. This reduced problem, in the form of the nonlinear algebraic system of (4.13), now involves the regular part of the Bloch Green's function for the reduced-wave operator. This Green's function, which is required to obtain a highly accurate stability threshold, was not considered in [**10**]. In §5.3 of [**10**] only a two-term expansion in ν for the stability threshold was obtained.

For both the Schnakenberg and GS models, we show that our hybrid method provides a significantly more accurate determination of the stability threshold than the two-term expansions of [**10**] when ε is only moderately small. In contrast to the earlier analyses in [**30**], [**12**], and [**24**], for summing infinite logarithmic for the eigenvalues of the Laplacian in 2-D domain with small holes, the main novelty of our analysis is that the local behaviour of the spot profile satisfies a nonlinear, rather than a linear, problem. In addition, as mentioned above, the implementation of our hybrid method for accurately calculating stability thresholds requires obtaining a tractable analytical expression for the regular part of the Bloch Green's function for either the Laplacian or reduced wave-operator. In the study of wave-scattering by arrays of cylinders, the numerical computation of the Bloch Green's functions is well-known to be a challenging problem owing to the very slow convergence of their infinite series representations in the spatial domain. Methodologies to improve the convergence properties based on the Poisson summation formula are surveyed in [**17**] and [**18**]. In §6 of [**10**] an Ewald-summation approach, motivated by the analysis of [**3**], was used to derive a computationally tractable explicit formula for the regular part of the Bloch Green's function for the Laplacian. This explicit formula involves two rapidly converging infinite series, one each over the direct and reciprocal lattices associated with the periodic pattern. In §5.1, we extend this methodology to derive a similar formula for the regular part of the Bloch Green's function for the reduced-wave operator, which is required for an accurate determination of the competition stability threshold for the GS model given in §5.2. The paper concludes with brief discussion in §6.

2 Lattices and the Bloch Green's Functions

In this section we recall a few basic facts about lattices and we introduce the Bloch Green's function for the reduced-wave operator that plays a central role in the analysis in §4.

Let $\boldsymbol{l}_1$ and $\boldsymbol{l}_2$ be two linearly independent vectors in $\mathbb{R}^2$, with angle θ between them, where without loss of generality we take $\boldsymbol{l}_1$ to be aligned with the positive x-axis. The Bravais lattice Λ is defined by

$$\Lambda = \left\{ m\boldsymbol{l}_1 + n\boldsymbol{l}_2 \,\middle|\, m, n \in \mathbb{Z} \right\}, \tag{2.1}$$

where $\mathbb{Z}$ denotes the set of integers. The *primitive* cell is the parallelogram generated by the vectors $\boldsymbol{l}_1$ and $\boldsymbol{l}_2$ of area

$|\boldsymbol{l}_1 \times \boldsymbol{l}_2|$. In particular, for a regular hexagonal lattice with a unit area for the primitive cell we have $\boldsymbol{l}_1 = \left(\left(\frac{4}{3}\right)^{1/4}, 0 \right)$ and $\boldsymbol{l}_2 = \left(\frac{4}{3}\right)^{1/4} \left(\frac{1}{2}, \frac{\sqrt{3}}{2} \right)$. In Fig. 1 we plot a portion of this hexagonal lattice.
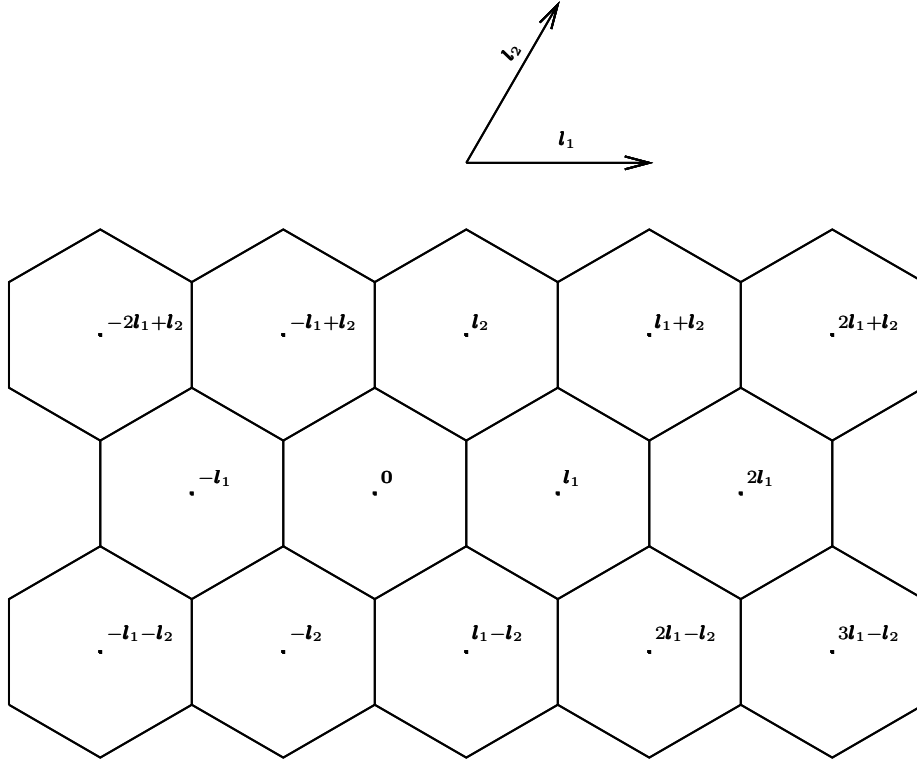
Figure 1. A regular hexagonal lattice. The fundamental Wigner-Seitz (WS) cell Ω for this lattice is the regular hexagon centred at the origin.

The *Wigner-Seitz (WS) or Voronoi cell* centred at a given lattice point of Λ consists of all points in the plane that are closer to this point than to any other lattice point. It is well-known that the WS cell is a convex polygon with the same area $|\boldsymbol{l}_1 \times \boldsymbol{l}_2|$ of the primitive cell, and that the union of the WS cells for an arbitrary oblique Bravais lattice tile all of $\mathbb{R}^2$ (cf. [2]) so that $\mathbb{R}^2 = \bigcup_{z \in \Lambda}(z + \Omega)$, where Ω is the WS cell centred at the origin, referred to as the fundamental WS cell. In Fig. 1 we show this fundamental WS cell for the regular hexagonal lattice.

As in [3], we define the reciprocal lattice $\Lambda^\star$ in terms of reciprocal vectors $\boldsymbol{d}_1$ and $\boldsymbol{d}_2$ by

$$(2.2) \qquad \Lambda^\star = \left\{ m\boldsymbol{d}_1 + n\boldsymbol{d}_2 \,\middle|\, m, n \in \mathbb{Z} \right\}, \qquad \text{where} \quad \boldsymbol{d}_i \cdot \boldsymbol{l}_j = \delta_{ij} \,,$$

where δ_{ij} is the Kronecker symbol. The first Brillouin zone, labelled by Ω_B, is the WS cell centred at the origin in the reciprocal space. Other authors (cf. [17], [18]) define the reciprocal lattice as $\Lambda^\star = \{2\pi m\, \boldsymbol{d}_1, 2\pi n\, \boldsymbol{d}_2\}_{m,n \in \mathbb{Z}}$. Our choice (2.2) for $\Lambda^\star$ is motivated by the form of the Poisson summation formula of [3] given in (5.4) below, and which is used in § 5.1 to numerically compute a required Bloch Green's function.

A more precise characterization of the fundamental WS cell, as required below in §2.1, is as follows. We first observe that there are eight nearest neighbour lattice points to $\mathbf{x} = 0$ given by the set

$$(2.3) \qquad P \equiv \left\{ m\boldsymbol{l}_1 + n\boldsymbol{l}_2 \,|\, m \in \{0, 1, -1\}, \; n \in \{0, 1, -1\}, \; (m, n) \neq 0 \right\}.$$

For each (vector) point $\boldsymbol{P}_i \in P$, for $i = 1, \ldots, 8$, we define a Bragg line L_i. This is the line that crosses the point $\boldsymbol{P}_i/2$ orthogonally to $\boldsymbol{P}_i$. We define the unit outer normal to L_i by $\boldsymbol{\eta}_i \equiv \boldsymbol{P}_i/|\boldsymbol{P}_i|$. The convex hull generated by these Bragg lines is the fundamental WS cell Ω, and the boundary $\partial\Omega$ of this cell is, generically, the union of six Bragg lines. For a square lattice, $\partial\Omega$ has four Bragg lines. The centres of the Bragg lines generating $\partial\Omega$ are re-indexed as $\boldsymbol{P}_i$ for $i = 1, \ldots, L$, where $L \in \{4, 6\}$ is the number of Bragg lines de-marking $\partial\Omega$. The boundary $\partial\Omega$ of Ω is the union of the re-indexed Bragg lines L_i, for $i = 1, \ldots, L$, and is parametrized segment-wise by a parameter t as

$$(2.4) \qquad \partial\Omega = \left\{ \mathbf{x} \in \bigcup_i \{ \frac{\boldsymbol{P}_i}{2} + t\boldsymbol{\eta}_i^{\perp} \} \ \middle| \ -t_i \le t \le t_i, \ \ i = 1, \ldots, L, \ \ L = \{4, 6\} \right\}.$$

Here $2t_i$ is the length of L_i, and $\boldsymbol{\eta}_i^{\perp}$ is the direction perpendicular to $\boldsymbol{P}_i$, and therefore tangent to L_i.

An important consequence of this construction is that Bragg lines on $\partial\Omega$ must come in pairs. In other words, suppose that $\boldsymbol{P}$ is a neighbour of 0 and that the Bragg line crossing $\boldsymbol{P}/2$ lies on $\partial\Omega$. Then, by symmetry, the Bragg line crossing $-\boldsymbol{P}/2$ must also lie on $\partial\Omega$.

2.1 The Bloch Green's Function for the Reduced-Wave Operator

In our analysis of the stability of spot patterns for the GS model in § 4 below, the Bloch Green's function $G_b(\mathbf{x})$ for the reduced-wave operator plays a prominent role. It satisfies

$$(2.5\,a) \qquad \Delta G_b - \frac{1}{D} G_b = -\delta(\mathbf{x}),$$

subject to the quasi-periodicity condition on $\mathbb{R}^2$ that

$$(2.5\,b) \qquad G_b(\mathbf{x} + \boldsymbol{l}) = e^{-i\boldsymbol{k}\cdot\boldsymbol{l}} \, G_b(\mathbf{x}), \qquad \boldsymbol{l} \in \Lambda,$$

where Λ is the Bravais lattice (2.1). As we show below, (2.5 b) indirectly yields boundary conditions on the boundary $\partial\Omega$ of the WS cell. The regular part $R_b(\boldsymbol{k})$ of this Bloch Green's function is defined by

$$(2.5\,c) \qquad R_b(\boldsymbol{k}) \equiv \lim_{\mathbf{x} \to \mathbf{0}} \left(G_b(\mathbf{x}) + \frac{1}{2\pi} \log |\mathbf{x}| \right).$$

A key result, as needed in §4, is that $R_b(\boldsymbol{k})$ is real-valued. A similar result for the regular part of the Bloch Green's function for the Laplacian was proved in Lemma 2.1 of [**10**]. For completeness, we give the simple proof here.

Lemma 2.1 *The regular part $R_b(\boldsymbol{k})$ of the Bloch Green's function $G_b(\mathbf{x})$ satisfying (2.5) is real-valued.*

<u>Proof:</u> Let $0 < \rho \ll 1$ and define $\Omega_\rho \equiv \Omega - B_\rho(0)$, where $B_\rho(0)$ is the ball of radius ρ centred at $\mathbf{x} = 0$. We multiply (2.5 a) by $\bar{G}_b$, where the bar denotes conjugation, and integrate over Ω_ρ. Upon using the divergence theorem we get

$$(2.6) \qquad \int_{\Omega_\rho} \bar{G}_b \Delta G_b \, d\mathbf{x} + \int_{\Omega_\rho} \nabla \bar{G}_b \cdot \nabla G_b \, d\mathbf{x} = \int_{\partial\Omega_\rho} \bar{G}_b \, \partial_n G_b \, d\mathbf{x} = \int_{\partial\Omega} \bar{G}_b \, \partial_n G_b \, d\mathbf{x} - \int_{\partial B_\rho(0)} \bar{G}_b \, \partial_{|\mathbf{x}|} G_b \, d\mathbf{x},$$

where $\partial_n G_b$ denotes the outward normal derivative of G_b on $\partial\Omega$. For $\rho \ll 1$, we use (2.5 c) to calculate

$$(2.7) \qquad \int_{\partial B_\rho(0)} \bar{G}_b \, \partial_{|\mathbf{x}|} G_b \, d\mathbf{x} \sim \int_0^{2\pi} \left(-\frac{1}{2\pi} \log \rho + R_b(\boldsymbol{k}) + o(1) \right) \left(-\frac{1}{2\pi\rho} + \mathcal{O}(1) \right) \rho \, d\theta \sim \frac{1}{2\pi} \log \rho - R_b(\boldsymbol{k}) + \mathcal{O}(\rho \log \rho).$$

Next, we use (2.7), together with $\Delta G_b = G_b/D$ in Ω_ρ, in (2.6). Upon letting $\rho \to 0$ we obtain

$$(2.8) \qquad R_b(\boldsymbol{k}) = -\int_{\partial\Omega} \bar{G}_b(\mathbf{x})\,\partial_n G_b(\mathbf{x})\,d\mathbf{x} + \lim_{\rho\to 0}\Big[\int_{\Omega_\rho} \Big(|\nabla G_b|^2 + \frac{1}{D}|G_b|^2 \Big)\,d\mathbf{x} + \frac{1}{2\pi}\log\rho\Big].$$

To establish that $R_b(\boldsymbol{k})$ is real-valued it suffices to show that the boundary integral term in (2.8) vanishes. To prove this, we observe that since the Bragg lines come in pairs, we have

$$(2.9) \qquad \int_{\partial\Omega} \bar{G}_b(\mathbf{x})\,\partial_n G_b(\mathbf{x})\,d\mathbf{x} = \sum_{i=1}^{L/2}\left(\int_{\frac{\boldsymbol{P}_i}{2}+t\boldsymbol{\eta}_i^\perp} \bar{G}_b(\mathbf{x})\nabla_{\mathbf{x}}G_b(\mathbf{x})\cdot\boldsymbol{\eta}_i\,d\mathbf{x} - \int_{\frac{-\boldsymbol{P}_i}{2}+t\boldsymbol{\eta}_i^\perp} \bar{G}_b(\mathbf{x})\nabla_{\mathbf{x}}G_b(\mathbf{x})\cdot\boldsymbol{\eta}_i\,d\mathbf{x}\right).$$

Here we have used the fact that the outward normals to the Bragg line pairs $\boldsymbol{P}_i/2 + t\boldsymbol{\eta}_i^\perp$ and $-\boldsymbol{P}_i/2 + t\boldsymbol{\eta}_i^\perp$ are in opposite directions. We then translate $\mathbf{x}$ by $\boldsymbol{P}_i$ to get

$$(2.10) \quad \int_{\frac{\boldsymbol{P}_i}{2}+t\boldsymbol{\eta}_i^\perp} \bar{G}_b(\mathbf{x})\nabla_{\mathbf{x}}G_b(\mathbf{x})\cdot\boldsymbol{\eta}_i\,d\mathbf{x} = \int_{\frac{-\boldsymbol{P}_i}{2}+t\boldsymbol{\eta}_i^\perp+\boldsymbol{P}_i} \bar{G}_b(\mathbf{x})\nabla_{\mathbf{x}}G_b(\mathbf{x})\cdot\boldsymbol{\eta}_i\,d\mathbf{x} = \int_{\frac{-\boldsymbol{P}_i}{2}+t\boldsymbol{\eta}_i^\perp} \bar{G}_b(\mathbf{x}+\boldsymbol{P}_i)\nabla_{\mathbf{x}}G_b(\mathbf{x}+\boldsymbol{P}_i)\cdot\boldsymbol{\eta}_i\,d\mathbf{x}.$$

Then, since $\boldsymbol{P}_i \in \Lambda$, we have by the quasi-periodicity condition (2.5 b) that

$$\bar{G}_b(\mathbf{x}+\boldsymbol{P}_i)\nabla_{\mathbf{x}}G_b(\mathbf{x}+\boldsymbol{P}_i) = \Big(\bar{G}_b(\mathbf{x})e^{i\boldsymbol{k}\cdot\boldsymbol{P}_i}\Big)\Big(\nabla_{\mathbf{x}}G_b(\mathbf{x})e^{-i\boldsymbol{k}\cdot\boldsymbol{P}_i}\Big) = \bar{G}_b(\mathbf{x})\nabla_{\mathbf{x}}G_b(\mathbf{x}).$$

Therefore, from (2.10) we conclude that

$$\int_{\frac{\boldsymbol{P}_i}{2}+t\boldsymbol{\eta}_i^\perp} \bar{G}_b(\mathbf{x})\nabla_{\mathbf{x}}G_b(\mathbf{x})\cdot\boldsymbol{\eta}_i\,d\mathbf{x} = \int_{\frac{-\boldsymbol{P}_i}{2}+t\boldsymbol{\eta}_i^\perp} \bar{G}_b(\mathbf{x})\nabla_{\mathbf{x}}G_b(\mathbf{x})\cdot\boldsymbol{\eta}_i\,d\mathbf{x},$$

which establishes from (2.9) that $\int_{\partial\Omega} \bar{G}_b(\mathbf{x})\,\partial_n G_b(\mathbf{x})\,d\mathbf{x} = 0$. From (2.8) we conclude that $R_b(\boldsymbol{k})$ is real. ∎

In §3 and §4 below, we will analyze the spectrum of the linearization around a steady-state periodic spot pattern for the Schnakenberg and GS models, respectively. For $\varepsilon \to 0$, it is the eigenfunction Ψ corresponding to the long-range solution component u that satisfies an elliptic PDE with coefficients that are spatially periodic on the lattice. As such, by the Floquet-Bloch theorem (cf. [15] and [13]), this eigenfunction must satisfy the quasi-periodic boundary conditions $\Psi(\mathbf{x}+\boldsymbol{l}) = e^{-i\boldsymbol{k}\cdot\boldsymbol{l}}\Psi(\mathbf{x})$ for $\boldsymbol{l} \in \Lambda$, $\mathbf{x} \in \mathbb{R}^2$ and $\boldsymbol{k}/(2\pi) \in \Omega_B$. This quasi-periodicity condition can be used to formulate a boundary operator on the boundary $\partial\Omega$ of the fundamental WS cell Ω. Let L_i and L_{-i} be two parallel Bragg lines on opposite sides of $\partial\Omega$ for $i = 1,\ldots,L/2$. Let $\mathbf{x}_{i1} \in L_i$ and $\mathbf{x}_{i2} \in L_{-i}$ be any two opposing points on these Bragg lines. We define the boundary operator $\mathcal{P}_{\boldsymbol{k}}\Psi$ by

$$(2.11) \quad \mathcal{P}_{\boldsymbol{k}}\Psi \equiv \left\{ \Psi \,\Big|\, \begin{pmatrix} \Psi(\mathbf{x}_{i1}) \\ \partial_n\Psi(\mathbf{x}_{i1}) \end{pmatrix} = e^{-i\boldsymbol{k}\cdot\boldsymbol{l}_i}\begin{pmatrix} \Psi(\mathbf{x}_{i2}) \\ \partial_n\Psi(\mathbf{x}_{i2}) \end{pmatrix}, \quad \forall\mathbf{x}_{i1}\in L_i,\ \forall\mathbf{x}_{i2}\in L_{-i},\ \boldsymbol{l}_i\in\Lambda,\ i=1,\ldots,L/2 \right\}.$$

The boundary operator $\mathcal{P}_0\Psi$ simply corresponds to a periodicity condition for Ψ on each pair of parallel Bragg lines. As such, $\mathcal{P}_0$ is the periodic boundary operator. These boundary operators are used in §3 and §4 below.

3 The Stability of Periodic Spot Patterns for the Schnakenberg Model

In this section we derive a new nonlinear algebraic system that accurately determines the competition stability threshold for a periodic pattern of spots for the Schnakenberg model, with an error that is smaller than any power of $\nu \equiv -1/\log\varepsilon$. The previous analysis in [10] provided only a two-term expansion of the competition stability threshold. The simplified form of the Schnakenberg model, considered in [11], is

$$(3.1) \qquad v_t = \varepsilon^2\Delta v - v + uv^2, \qquad \tau u_t = D\Delta u + a - \varepsilon^{-2}uv^2,$$

where $0 < \varepsilon \ll 1$, $D > 0$, $\tau > 0$, and $a > 0$, are parameters. We first use the method of matched asymptotic expansions to calculate a steady-state spot solution to (3.1) in the fundamental WS cell Ω centred at $\mathbf{x} = 0$ subject to periodic boundary conditions on $\partial\Omega$.

In the inner region near $\mathbf{x} = 0$ we look for a locally radially symmetric steady-state solution to (3.1) of the form

$$(3.2) \qquad u = \frac{1}{\sqrt{D}} U \,, \qquad v = \sqrt{D} V \,, \qquad \mathbf{y} = \varepsilon^{-1} \mathbf{x} \,.$$

Upon, substituting (3.2) into the steady-state equations of (3.1), we obtain that $V \sim V(\rho)$ and $U \sim U(\rho)$, with $\rho = |\mathbf{y}|$, satisfy the following inner, or core, problem:

$$(3.3\,a) \qquad \Delta_\rho V - V + U V^2 = 0 \,, \qquad \Delta_\rho U - U V^2 = 0 \,, \qquad 0 < \rho < \infty \,,$$

$$(3.3\,b) \qquad U'(0) = V'(0) = 0 \,; \qquad V \to 0 \,, \qquad U \sim S \log \rho + \chi(S) + o(1) \,, \quad \text{as} \quad \rho \to \infty \,,$$

where the unknown source strength $S \equiv \int_0^\infty U V^2 \rho \, d\rho$ is to be determined. Here we have defined $\Delta_\rho V \equiv V'' + \rho^{-1} V'$.

In [10], the following two-term expansion for the solution to (3.3) in the limit $S \to 0$ was calculated:

Lemma 3.1 *[see Lemma 5.1 of [10]]; For $S \to 0$, the asymptotic solution to the core problem (3.3) is*

$$V \sim \frac{S}{b} w + \frac{S^3}{b^3} \left(-\chi_1 b w + V_{1p} \right) + \cdots \,, \qquad U \sim \frac{b}{S} + S \left(\chi_1 + \frac{U_{1p}}{b} \right) + \cdots \,,$$

$$(3.4)$$

$$\chi \sim \frac{b}{S} + S \chi_1 + \cdots \,; \qquad \chi_1 \equiv \frac{1}{b^2} \int_0^\infty V_{1p} \rho \, d\rho \,.$$

Here $w(\rho)$ is the unique positive ground-state solution to $\Delta_\rho w - w + w^2 = 0$ and $b \equiv \int_0^\infty w^2 \rho d\rho$. In terms of $w(\rho)$, and the linear operator $L_0 V_{1p} \equiv \Delta_\rho V_{1p} - V_{1p} + 2w V_{1p}$, the functions $U_{1p}(\rho)$ and $V_{1p}(\rho)$ are the unique solutions to

$$L_0 V_{1p} = -w^2 U_{1p} \,, \quad 0 \le \rho < \infty \,; \qquad V'_{1p}(0) = 0 \,, \quad V_{1p} \to 0 \,, \quad \text{as} \quad \rho \to \infty \,,$$

$$(3.5)$$

$$\Delta_\rho U_{1p} = w^2 \,, \quad 0 \le \rho < \infty \,; \qquad U'_{1p}(0) = 0 \,, \quad U_{1p} \sim b \log \rho + o(1) \,, \quad \text{as} \quad \rho \to \infty \,; \qquad b \equiv \int_0^\infty w^2 \rho \, d\rho \,.$$

Numerical computations yield $b \approx 4.93$ and $\int_0^\infty V_{1p} \rho \, d\rho \approx 0.473$, so that $\chi_1 \approx 0.0194$.
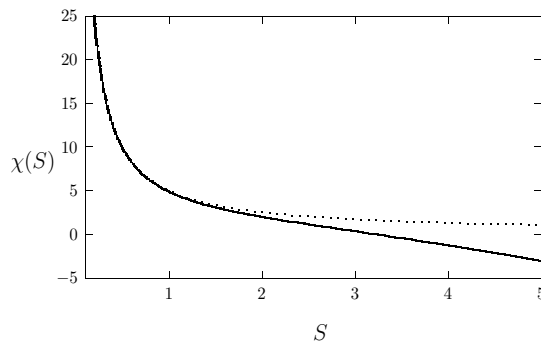
Figure 2. Plot of $\chi(S)$ (heavy solid curve), computed numerically from (3.3), and the two-term approximation (3.4) for $\chi(S)$ (dotted curve) valid for $S \ll 1$. They agree rather favorably on the range $0 < S < 2$.

The derivation of this result is given in Appendix A of [10] and will not be repeated here. In Fig. 2 we plot $\chi(S)$,

as computed numerically from (3.3), and we compare it with the two-term approximation from (3.4), which is valid for $S \ll 1$. Our numerical results indicate that $\chi'(S) < 0$ and $\chi''(S) > 0$ at least on the range $0 < S < 4.3$. We recall from [**11**] that the spot profile is linearly unstable to locally non-radially symmetric perturbations, which triggers a nonlinear spot self-replication process, when $S > \Sigma_2 \approx 4.3$. As such, in our analysis below we require that $S < \Sigma_2$.

The source strength S is determined by matching the far-field behaviour of the core solution to an outer solution for u valid away from $\mathcal{O}(\varepsilon)$ distances from the origin. In the outer region, v is exponentially small, and from (3.2) we get $\varepsilon^{-2}uv^2 \to 2\pi\sqrt{D}S\delta(\mathbf{x})$. Therefore, from (3.1), the outer steady-state problem for u is

$$
\Delta u = -\frac{a}{D} + \frac{2\pi}{\sqrt{D}} S\,\delta(\mathbf{x})\,, \quad \mathbf{x} \in \Omega\,; \qquad \mathcal{P}_0 u = 0\,, \quad \mathbf{x} \in \partial\Omega\,,
$$

(3.6)

$$
u \sim \frac{1}{\sqrt{D}}\left[S\log|\mathbf{x}| + \chi(S) + \frac{S}{\nu}\right]\,, \quad \text{as} \quad \mathbf{x} \to 0\,,
$$

where $\nu \equiv -1/\log\varepsilon$ and Ω is the fundamental WS cell. Upon using the divergence theorem we identify S as

$$
S = \frac{a|\Omega|}{2\pi\sqrt{D}}\,.
$$

(3.7)

Then, we introduce the periodic source-neutral Green's function $G_{p0}(\mathbf{x})$ and its regular part R_{p0}, which satisfy

$$
\Delta G_{p0} = \frac{1}{|\Omega|} - \delta(\mathbf{x})\,, \quad \mathbf{x} \in \Omega\,; \qquad \mathcal{P}_0 G_{p0} = 0 \quad \mathbf{x} \in \partial\Omega\,,
$$

(3.8)

$$
G_{p0} \sim -\frac{1}{2\pi}\log|\mathbf{x}| + R_{p0} + o(1)\,, \quad \text{as} \quad \mathbf{x} \to 0\,; \qquad \int_\Omega G_{p0}\,d\mathbf{x} = 0\,.
$$

In terms of this Green's function, the solution to (3.6) is $u(x) = -2\pi D^{-1/2}\left[SG_{p0}(\mathbf{x};0) - u_c\right]$, where the constant u_c is given by $u_c \equiv [2\pi\nu]^{-1}\left[S + 2\pi\nu SR_{p0} + \nu\chi(S)\right]$. An explicit expression for R_{p0} on a Bravais lattice Λ was derived in Theorem 1 of [**4**]. A steady-state periodic pattern of spots is then obtained through periodic extension to $\mathbb{R}^2$ of the one-spot solution constructed in Ω.

In Theorem 2 of [**4**] it was proved that, within the class of oblique Bravais lattices with unit area of the primitive cell, R_{p0} is minimized for a regular hexagonal lattice. For the class of lattices Λ for which $|\boldsymbol{l}_1| = |\boldsymbol{l}_2|$, we let $\boldsymbol{l}_1 = (1/\sqrt{\sin(\theta)}, 0)$ and $\boldsymbol{l}_2 = (\cos(\theta)/\sqrt{\sin(\theta)}, \sqrt{\sin(\theta)})$, where θ is the angle with respect to the horizontal axis. For this choice, the area $|\Omega|$ of the fundamental WS cell is $|\Omega| = 1$. Then, from Theorem 1 of [**4**], R_{p0} is given explicitly by

$$
R_{p0} = -\frac{1}{2\pi}\ln(2\pi) - \frac{1}{2\pi}\ln\left|\sqrt{\sin\theta}\,e^{\pi i\xi/6}\prod_{n=1}^{\infty}\left(1 - e^{2\pi in\xi}\right)^2\right|\,, \quad \xi = e^{i\theta}\,.
$$

(3.9)

In Fig. 3 we plot R_{p0} versus θ for this class of lattices. For a regular hexagon, where $\theta = \pi/3$, we have $R_{p0} \approx -0.21027$.

To study the linear stability of the periodic spot pattern with respect to fast $\mathcal{O}(1)$ time-scale instabilities, we use the Floquet-Bloch theorem that allows us to restrict the analysis to the fundamental WS cell Ω, provided we impose quasi-periodic boundary conditions on $\partial\Omega$. Upon introducing the perturbation

$$
u = u_e + e^{\lambda t}\eta\,, \qquad v = v_e + e^{\lambda t}\phi\,,
$$

(3.10)

in (3.1), where u_e and v_e denote the steady-state solution, we obtain a singularly perturbed eigenvalue problem for ϕ and η on Ω, which is formulated in terms of the quasi-periodic boundary operator $\mathcal{P}_{\boldsymbol{k}}$ of (2.11) as

$$
\varepsilon^2\Delta\phi - \phi + 2u_e v_e\phi + v_e^2\eta = \lambda\phi\,, \quad \mathbf{x} \in \Omega\,; \qquad \mathcal{P}_{\boldsymbol{k}}\phi = 0\,, \quad \mathbf{x} \in \partial\Omega\,,
$$

(3.11)

$$
D\Delta\eta - 2\varepsilon^{-2}u_e v_e\phi - \varepsilon^{-2}v_e^2\eta = \lambda\tau\eta\,, \quad \mathbf{x} \in \Omega\,; \qquad \mathcal{P}_{\boldsymbol{k}}\eta = 0\,, \quad \mathbf{x} \in \partial\Omega\,.
$$
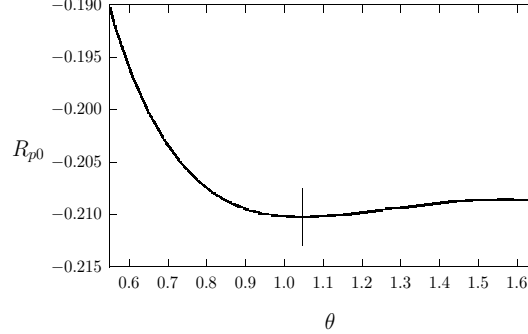
Figure 3. Plot of the the regular part R_{p0}, as given in (3.9) (cf. [4]), of the periodic source-neutral Green's function for oblique lattices of unit area for which $\boldsymbol{l}_1 = (1/\sqrt{\sin(\theta)}, 0)$ and $\boldsymbol{l}_2 = (\cos(\theta)/\sqrt{\sin(\theta)}, \sqrt{\sin(\theta)})$, so that $|\boldsymbol{l}_1| = |\boldsymbol{l}_2|$ and $|\Omega| = 1$. The vertical line denotes the hexagonal lattice for which $\theta = \pi/3$. The minimum occurs for the hexagon.

In the inner region near $\mathbf{x} = 0$ we introduce the local variables $N(\rho)$ and $\Phi(\rho)$ by

$$(3.12) \qquad \eta = \frac{1}{D} N(\rho), \qquad \phi = \Phi(\rho), \qquad \rho = |\mathbf{y}|, \qquad \mathbf{y} = \varepsilon^{-1}\mathbf{x}.$$

Upon substituting (3.12) into (3.11), and by using $u_e \sim U(\rho)/\sqrt{D}$ and $v_e \sim \sqrt{D}V(\rho)$, where U and V satisfy the core problem (3.3), we obtain on $0 < \rho < \infty$ that

$$(3.13) \qquad \begin{aligned} \Delta_\rho \Phi - \Phi + 2UV\Phi + NV^2 = \lambda\Phi, \qquad & \Phi \to 0, \quad \text{as} \quad \rho \to \infty; \qquad \Phi'(0) = 0, \\ \Delta_\rho N = 2UV\Phi + NV^2, \qquad & N \sim C\left[\log\rho + B\right], \quad \text{as} \quad \rho \to \infty; \qquad N'(0) = 0. \end{aligned}$$

Here $C = \int_0^\infty \left(2UV\Phi + NV^2\right) \rho \, d\rho$ is a normalization constant, and $B = B(S; \lambda)$ is determined as part of the solution to (3.13). A key observation, as obtained by comparing (3.13) with (3.3), is that at $\lambda = 0$ we have

$$(3.14) \qquad \Phi = C\partial_S V, \qquad N = C\partial_S U, \qquad B(S, 0) = \chi'(S).$$

To formulate the outer problem, we use the fact that v_e is localized to calculate in the sense of distributions that $\varepsilon^{-2}\left(2u_e v_e \phi + \eta v_e^2\right) \to \left(\int_{\mathbb{R}^2}\left(2UV\Phi + NV^2\right) d\mathbf{y}\right) \delta(\mathbf{x}) = 2\pi C\delta(\mathbf{x})$. By combining this expression with (3.11), and labelling $\nu = -1/\log\varepsilon$, we obtain that the outer problem for η is

$$(3.15) \qquad \begin{aligned} \Delta\eta - \frac{\tau\lambda}{D}\eta = \frac{2\pi C}{D}\delta(\mathbf{x}), \qquad & \mathbf{x} \in \Omega; \qquad \mathcal{P}_{\boldsymbol{k}}\eta = 0, \quad \mathbf{x} \in \partial\Omega, \\ \eta \sim \frac{C}{D}\left(\log|\mathbf{x}| + \frac{1}{\nu} + B\right), \qquad & \text{as} \quad \mathbf{x} \to 0. \end{aligned}$$

At the competition instability threshold, corresponding to the zero-eigenvalue crossing, we set $\lambda = 0$ in (3.15) and then write the solution to (3.15) for $\boldsymbol{k} \in \Omega_B/(2\pi)$ with $\boldsymbol{k} \neq 0$ as

$$(3.16) \qquad \eta(\mathbf{x}) = -\frac{2\pi C}{D}G_{b0}(\mathbf{x}),$$

where $G_{b0}(\mathbf{x})$ is the Bloch Green's function for the Laplacian defined for $\boldsymbol{k} \neq 0$ and $\boldsymbol{k} \in \Omega_B/(2\pi)$ by

$$(3.17) \qquad \begin{aligned} \Delta G_{b0} = -\delta(\mathbf{x}), \qquad & \mathbf{x} \in \Omega; \qquad \mathcal{P}_{\boldsymbol{k}}G_{b0} = 0, \quad \mathbf{x} \in \partial\Omega, \\ G_{b0} \sim -\frac{1}{2\pi}\log|\mathbf{x}| + R_{b0}(\boldsymbol{k}) + o(1), \qquad & \text{as} \quad \mathbf{x} \to 0. \end{aligned}$$

Here $R_{b0}(\boldsymbol{k})$ is the regular part of G_{b0}. In Lemma 2.1 of [10] it was proved that $R_{b0}(\boldsymbol{k})$ is real-valued, while in Lemma 2.2 of [10] it was proved that $R_{b0}(\boldsymbol{k}) \sim \left[\boldsymbol{k}^T \mathcal{Q}\boldsymbol{k}\right]^{-1}$ as $|\boldsymbol{k}| \to 0$, for some positive definite matrix $\mathcal{Q}$.

In §6 of [10], an analytical expression for $R_{b0}(\boldsymbol{k})$ when $\boldsymbol{k} \neq 0$ and $\boldsymbol{k} \in \Omega_B/(2\pi)$ was derived by adapting the

procedure used in [3] for the Helmholtz operator. The resulting expression consists of two infinite sums, one each over the direct and reciprocal lattice, and is given by

$$(3.18) \qquad R_{b0}(\boldsymbol{k}) = \sum_{\boldsymbol{d} \in \Lambda^\star} \exp\left(-\frac{|2\pi\boldsymbol{d} - \boldsymbol{k}|^2}{4\eta^2}\right) \frac{1}{|2\pi\boldsymbol{d} - \boldsymbol{k}|^2} + \frac{1}{4\pi} \sum_{\substack{\boldsymbol{l} \in \Lambda \\ \boldsymbol{l} \neq \boldsymbol{0}}} e^{i\boldsymbol{k}\cdot\boldsymbol{l}} E_1(|\boldsymbol{l}|^2\eta^2) - \frac{\gamma}{4\pi} - \frac{\log\eta}{2\pi},$$

where $\gamma = 0.57721\cdots$ is Euler's constant and $E_1(z) = \int_z^\infty t^{-1}e^{-t}\, dt$ is the exponential integral (cf. §5.1.1 of [1]). In (3.18), $\eta > 0$ is a cutoff parameter chosen to ensure that both infinite sums have good convergence properties.

Finally, upon expanding (3.16) as $\mathbf{x} \to 0$, and then comparing the resulting expression with the required singular behaviour $\eta \sim CD^{-1}(\log|\mathbf{x}| + \nu^{-1} + B)$ from (3.15), we conclude at $\lambda = 0$ that

$$(3.19) \qquad \frac{1}{\nu} + \chi'(S) = -2\pi R_{b0}(\boldsymbol{k}), \qquad S = \frac{a|\Omega|}{2\pi\sqrt{D}}, \qquad \nu \equiv -1/\log\varepsilon.$$

This nonlinear algebraic equation, not derived in [10], determines the competition instability threshold with an error that is smaller than any power of ν.

To compare stability thresholds on different lattices, we fix the area of the fundamental WS cell as $|\Omega| = 1$. For a given lattice Λ, (3.19) is an implicit equation determining critical values $D(\boldsymbol{k})$ of D for which $\lambda = 0$ is in the spectrum of the linearization as $2\pi\boldsymbol{k}$ is varied in the first Brillouin zone. Since $\chi''(S) > 0$, and S is inversely proportional to D, it follows that the minimum value $D^\star$ of $D(\boldsymbol{k})$ is determined by the minimum value $R_{b0}^\star$, defined by $R_{b0}^\star = \min_{\boldsymbol{k}\in\Omega_B/(2\pi)} R_{b0}(\boldsymbol{k})$. The critical value $D^\star$ determines the competition stability threshold for a given lattice Λ. Finally, to determine the lattice arrangement with the largest stability threshold, i.e. that maximizes $D^\star$, we simply define $\mathcal{K}_s^\star$ by

$$(3.20) \qquad \mathcal{K}_s^\star \equiv \max_\Lambda R_{b0}^\star, \qquad R_{b0}^\star = \min_{\boldsymbol{k}\in\Omega_B/(2\pi)} R_{b0}(\boldsymbol{k}).$$

Then, to within all powers of ν, the optimal stability threshold D_{opt} is the root of the nonlinear algebraic equation

$$(3.21) \qquad \frac{1}{\nu} + \chi'(S) = -2\pi\mathcal{K}_s^\star, \qquad S = \frac{a}{2\pi\sqrt{D_{\mathrm{opt}}}}, \qquad \nu \equiv -1/\log\varepsilon.$$

To determine a two-term expansion for the root to (3.21) when $\nu \ll 1$, we simply substitute the two-term expansion for $\chi(S)$ as $S \to 0$, as given in (3.4), and solve for D_{opt}. In this way, we obtain the two-term asymptotic expansion

$$(3.22) \qquad D_{\mathrm{opt},2} \equiv \frac{a^2}{4\pi^2 b\nu}\left[1 + \nu\left(2\pi\mathcal{K}_s^\star + \chi_1\right) + \mathcal{O}(\nu^2)\right],$$

in powers of ν, for D_{opt}, where χ_1 and b are defined in (3.4). This two-term result was derived previously in [10].

This simple analytical method, which relies critically on the observation that $B = \chi'(S)$ at $\lambda = 0$, provides a rather expedient approach for calculating the optimal competition instability threshold in D. However, it does not characterize the spectrum contained in the small ball $|\lambda| = \mathcal{O}(\nu) \ll 1$ near the origin when D is near the leading-order stability threshold $a^2/(4\pi^2 b\nu)$. This latter, more refined, analysis is given in §3 of [10].

From the numerical computations in §6.1 of [10], based on the explicit formula (3.18) for $R_{b0}(\boldsymbol{k})$, it was shown in [10] that $R_{b0}^\star$ is maximized for a regular hexagonal lattice. From Table 2 of [10], we identify $\mathcal{K}_s^\star \approx -0.079124$, corresponding to this hexagonal lattice. On this optimal hexagonal lattice, we set $a = 1$, and in Fig. 4 we compare, for a range of ν values, the two-term result for the stability threshold (3.22) with the corresponding result, accurate to all orders in ν, computed numerically from (3.21). In solving the nonlinear algebraic equation (3.21) we computed $\chi'(S)$ from the numerical solution to the core problem (3.3). We observe from Fig. 4 that the two-term expansion (3.22) is accurate only for relatively small ν. In fact, for $\varepsilon = 0.02$ the two-term result over-estimates the threshold
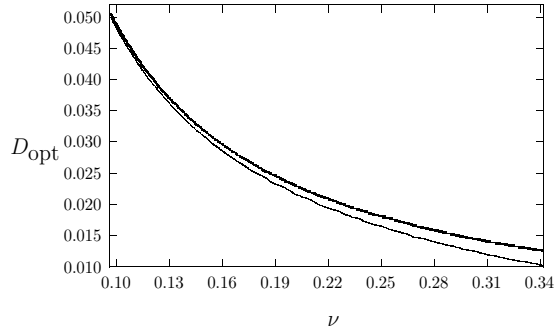
Figure 4. Plot of the optimal stability threshold D_{opt} on a hexagonal lattice versus ν for the Schnakenberg model with $a = 1$. The range $0.096 < \nu < 0.34$, corresponds to $0.3 \times 10^{-4} < \varepsilon < 0.0528$. The heavy solid curve is the two-term result (3.22). The solid curve is the result computed from (3.21) that is accurate to all powers of ν. For $\varepsilon = .01$, $\varepsilon = .02$, and $\varepsilon = .05$ there is a 7.6%, a 9.4%, and a 17%, difference, respectively, between these two results.
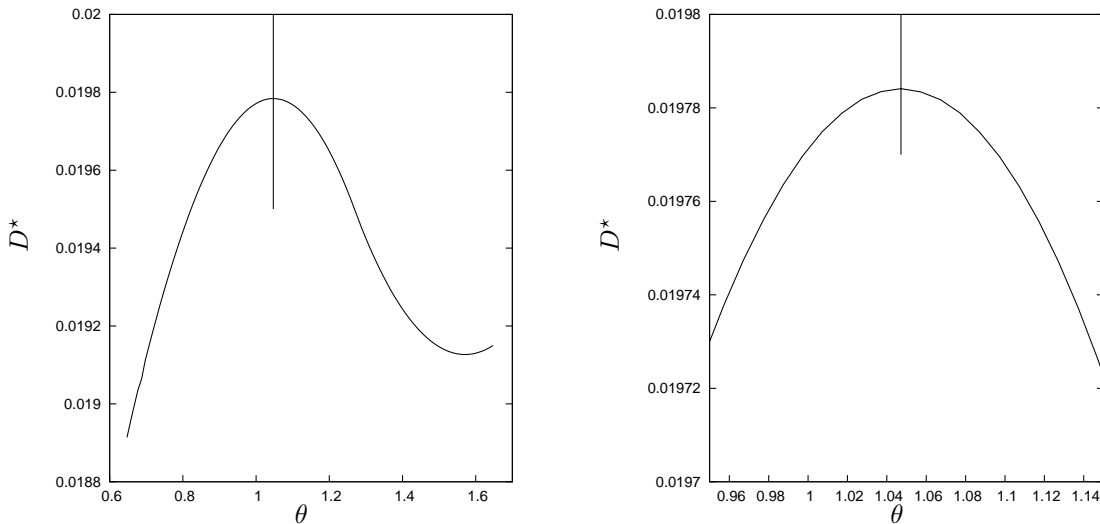
Figure 5. Plots of the stability threshold $D^\star$ for the Schnakenberg model with $a = 1$ and $\varepsilon = 0.01$ on a class of lattices with unit area, with primitive vectors $\boldsymbol{l}_1 = (1/\sqrt{\sin(\theta)}, 0)$ and $\boldsymbol{l}_2 = (\cos(\theta)/\sqrt{\sin(\theta)}, \sqrt{\sin(\theta)})$, where the parameter θ satisfies $0 < \theta < \pi/2$. This threshold $D^\star$ is computed from (3.19) where $R_{b0}(\boldsymbol{k})$ is replaced by $R_{b0}^\star \equiv \min_{\boldsymbol{k} \in \Omega_B/(2\pi)} R_{b0}(\boldsymbol{k})$. The vertical line at $\theta = \pi/3$ corresponds to the regular hexagonal lattice.

from the more accurate theory by approximately 9.4%. This suggests that at small but finite ε, the formulation (3.21) provides a considerably more accurate prediction for the stability threshold than the two-term result (3.22).

Next, we illustrate how the competition stability threshold for D varies with respect to the lattice. For simplicity, we consider the class of lattices Λ for which $|\boldsymbol{l}_1| = |\boldsymbol{l}_2|$ and $|\Omega| = 1$, where $\boldsymbol{l}_1 = (1/\sqrt{\sin(\theta)}, 0)$ and $\boldsymbol{l}_2 = (\cos(\theta)/\sqrt{\sin(\theta)}, \sqrt{\sin(\theta)})$ for $0 < \theta < \pi/2$. At each value of θ, we numerically compute $R_{b0}^\star$ by discretizing $\boldsymbol{k}$-space as in §6.1 of [10]. The stability threshold $D^\star$ versus θ is then obtained by solving (3.19) numerically, where we replace $R_{b0}(\boldsymbol{k})$ on the right-hand side of (3.19) with $R_{b0}^\star$. For $a = 1$ and $\varepsilon = 0.01$, corresponding to $\nu \approx 0.217$, in Fig. 5 we plot $D^\star$ versus θ. A zoom of this plot for θ near $\pi/3$, corresponding to the regular hexagonal lattice, is shown in the right panel of Fig. 5. As expected, the optimal threshold occurs for the hexagonal lattice.

4 The Stability of Periodic Spot Patterns for the Gray-Scott Model

In this section we formulate a new hybrid asymptotic-numerical method to determine an approximation, accurate to all orders in $\nu \equiv -1/\log \varepsilon$, for the optimal competition instability threshold for a periodic pattern of spots for the GS model. Previously in [10], a two-term expansion for the threshold was derived. In implementing our theory, we will need to analyze the Bloch Green's function for the reduced-wave operator, which was not considered in [10].

On the fundamental WS cell Ω, the GS model in the dimensionless form of [19] is

$$(4.1) \qquad v_t = \varepsilon^2 \Delta v - v + Auv^2, \quad \tau u_t = D\Delta u + (1-u) - uv^2, \quad \mathbf{x} \in \Omega; \qquad \mathcal{P}_0 u = \mathcal{P}_0 v = 0, \quad \mathbf{x} \in \partial\Omega,$$

where $\varepsilon > 0$, $D > 0$, $\tau > 1$, and the feed-rate parameter $A > 0$ are constants. Here $\mathcal{P}_0$ is the boundary operator corresponding to periodic boundary conditions on $\partial\Omega$, as defined in (2.11).

We first construct a one-spot steady-state solution to (4.1) with spot centred at $\mathbf{x} = 0$ in Ω in the regime $A = \mathcal{O}(\varepsilon)$ by using the approach in §2 of [5]. In the inner region we introduce the local variables U, V, and $\mathbf{y}$, defined by

$$(4.2) \qquad u = \frac{\varepsilon}{A\sqrt{D}} U, \qquad v = \frac{\sqrt{D}}{\varepsilon} V, \qquad \mathbf{y} = \varepsilon^{-1}\mathbf{x},$$

into the steady-state problem for (4.1). For $\varepsilon \ll 1$, we readily obtain that $U(\rho)$ and $V(\rho)$, with $\rho = |\mathbf{y}|$, satisfy the same core problem (3.3) as for the Schnakenberg model, where $S = \int_0^\infty UV^2 \rho\, d\rho$.

To formulate the outer problem for u, we observe that since v is localized near $\mathbf{x} = 0$ we have in the sense of distributions that $uv^2 \to \varepsilon^2 \left(\int_{\mathbb{R}^2} \sqrt{D} (A\varepsilon)^{-1} UV^2 \, d\mathbf{y} \right) \delta(\mathbf{x}) \sim 2\pi\varepsilon\sqrt{D}A^{-1}S\,\delta(\mathbf{x})$. Then, upon matching u to the inner core solution U, we obtain from the steady-state problem for (4.1) that

$$(4.3) \qquad \Delta u + \frac{1}{D}(1-u) = \frac{2\pi\varepsilon}{A\sqrt{D}} S\,\delta(\mathbf{x}), \quad \mathbf{x} \in \Omega; \qquad \mathcal{P}_0 u = 0, \quad \mathbf{x} \in \partial\Omega,$$

$$u \sim \frac{\varepsilon}{A\sqrt{D}} \left(S\log|\mathbf{x}| + \frac{S}{\nu} + \chi(S) \right), \quad \text{as} \quad \mathbf{x} \to 0,$$

where $\nu \equiv -1/\log \varepsilon$. The solution to (4.3) is $u = 1 - 2\pi\varepsilon SG_p(\mathbf{x})/(A\sqrt{D})$, where $G_p(\mathbf{x})$ is the periodic reduced-wave Green's function with regular part R_p satisfying

$$(4.4) \qquad \Delta G_p - \frac{1}{D}G_p = -\delta(\mathbf{x}), \quad \mathbf{x} \in \Omega; \qquad \mathcal{P}_0 G_p = 0, \quad \mathbf{x} \in \partial\Omega,$$

$$G_p(\mathbf{x}) \sim -\frac{1}{2\pi}\log|\mathbf{x}| + R_p + o(1), \quad \text{as} \quad \mathbf{x} \to 0.$$

By expanding u as $\mathbf{x} \to 0$ and comparing it with the required behaviour in (4.3), we obtain that S satisfies

$$(4.5) \qquad S + \nu\left[\chi(S) + 2\pi SR_p\right] = \frac{A\nu\sqrt{D}}{\varepsilon}.$$

To analyze the linear stability of the steady-state solution u_e and v_e, we introduce (3.10) into (4.1) to obtain the Floquet-Bloch eigenvalue problem

$$(4.6) \qquad \varepsilon^2 \Delta\phi - \phi + 2Au_e v_e \phi + Av_e^2 \eta = \lambda\phi, \quad \mathbf{x} \in \Omega; \qquad \mathcal{P}_{\boldsymbol{k}}\phi = 0, \quad \mathbf{x} \in \partial\Omega,$$

$$D\Delta\eta - \eta - 2u_e v_e \phi - v_e^2 \eta = \lambda\tau\eta; \quad \mathbf{x} \in \Omega; \qquad \mathcal{P}_{\boldsymbol{k}}\phi = 0, \quad \mathbf{x} \in \partial\Omega.$$

In the inner region near $\mathbf{x} = 0$ we look for a locally radially symmetric eigenpair of the form

$$(4.7) \qquad \eta = \frac{\varepsilon}{A\sqrt{D}} N(\rho), \qquad \phi = \frac{\sqrt{D}}{\varepsilon}\Phi(\rho), \qquad \rho = |\mathbf{y}|, \qquad \mathbf{y} = \varepsilon^{-1}\mathbf{x}.$$

From (4.6), we obtain to within negligible $\mathcal{O}(\varepsilon^2)$ terms that $N(\rho)$ and $\Phi(\rho)$ satisfy the same inner problem (3.13) as for the Schnakenberg model. To determine the outer problem for η, we calculate in the sense of distributions that

$2u_e v_e \phi + v_e^2 \eta \to \sqrt{D} A^{-1} \varepsilon \left[\int_{\mathbb{R}^2} \left(2UV\Phi + V^2 N \right) \, d\mathbf{y} \right] \delta(\mathbf{x}) = 2\pi \varepsilon \sqrt{D} A^{-1} C \delta(\mathbf{x})$. Then, by asymptotically matching η as $\mathbf{x} \to 0$ with the far-field behaviour of $N(\rho)$ in (3.13) as $\rho \to \infty$, we obtain from (4.6) that the outer problem is

(4.8)
$$\Delta \eta - \frac{(1 + \tau\lambda)}{D} \eta = \frac{2\pi\varepsilon}{A\sqrt{D}} C\delta(\mathbf{x}), \quad \mathbf{x} \in \Omega; \qquad \mathcal{P}_{\boldsymbol{k}} \eta = 0, \quad \mathbf{x} \in \partial\Omega,$$
$$\eta \sim \frac{\varepsilon C}{A\sqrt{D}} \left[\log |\mathbf{x}| + \frac{1}{\nu} + B \right], \quad \text{as} \quad \mathbf{x} \to 0,$$

where $B = B(S; \lambda)$ is to be computed from (3.13). We recall from (3.14) that $B = \chi'(S)$ at $\lambda = 0$.

At the competition instability threshold, corresponding to the zero eigenvalue crossing, we set $\lambda = 0$ in (4.8) and then write the solution to (4.8) as

(4.9)
$$\eta(x) = -\frac{2\pi\varepsilon C}{A\sqrt{D}} G_b(\mathbf{x}),$$

where $G_b(\mathbf{x})$ is the Bloch Green's function for the reduced-wave operator, as defined by (2.5). Then, by imposing that the behaviour of η as $\mathbf{x} \to 0$ agrees with that in (4.8), we obtain at $\lambda = 0$ that $C + 2\pi\nu C R_b(\boldsymbol{k}) + \nu B = 0$, where $R_b(\boldsymbol{k})$ is the regular part of $G_b(\mathbf{x})$, as defined in (2.5 c). Finally, upon setting $B = \chi'(S)$, and recalling (4.5) for the determination of S from the steady-state theory, we conclude at $\lambda = 0$ that

(4.10)
$$S + \nu \left[\chi(S) + 2\pi S R_p \right] = \frac{A\nu\sqrt{D}}{\varepsilon}, \qquad \frac{1}{\nu} + \chi'(S) = -2\pi R_b(\boldsymbol{k}).$$

In order to compare our results with those in [10], we introduce $\mathcal{A}$, ν, and D_0, defined by

(4.11)
$$\mathcal{A} = \frac{A}{\varepsilon} \sqrt{\frac{|\Omega|}{2\pi}}, \qquad D = \frac{D_0}{\nu}, \qquad \mu = \frac{2\pi D_0}{|\Omega|},$$

so that (4.10) becomes

(4.12)
$$S + \nu \left[\chi(S) + 2\pi S R_p \right] = \mathcal{A}\sqrt{\nu\mu}, \qquad \frac{1}{\nu} + \chi'(S) = -2\pi R_b(\boldsymbol{k}).$$

We first fix ε, D, and the lattice Λ with $|\Omega| = 1$, and we let $S(\boldsymbol{k})$ denote the root to the second equation in (4.12). Since $\chi''(S) > 0$, the left-hand side of this equation is monotone increasing, so that $S(k) < S^\star$, where $S^\star$ is the root of $\nu^{-1} + \chi'(S^\star) = -2\pi\nu R_b^\star$, where $R_b^\star = \min_{\boldsymbol{k} \in \Omega_B/(2\pi)} R_b(\boldsymbol{k})$. Then, since the left-hand side of the first equation in (4.12) is monotone increasing in S when $\nu \ll 1$, it follows for $\nu \ll 1$ that the largest value of $\mathcal{A}$ for which $\lambda = 0$ is in the spectrum of the linearization is given by

(4.13)
$$\mathcal{A}^\star = \frac{1}{\sqrt{\nu\mu}} \left(S^\star + \nu \left[\chi(S^\star) + 2\pi S^\star R_p \right] \right), \qquad \frac{1}{\nu} + \chi'(S^\star) = -2\pi R_b^\star.$$

This coupled nonlinear algebraic system, not derived in [10], determines the optimal competition instability threshold to within an error that is smaller than any power of ν.

We identify the optimal lattice as the one that minimizes $\mathcal{A}^\star$. To determine this optimum lattice we must minimize $S^\star$ and R_p with respect to the lattice Λ. As such we define $\mathcal{K}_{gs}^\star$ and $R_p^\star$ by

(4.14)
$$\mathcal{K}_{gs}^\star \equiv \max_\Lambda R_b^\star, \qquad R_b^\star \equiv \min_{\boldsymbol{k} \in \Omega_B/2\pi} R_b(\boldsymbol{k}); \qquad R_p^\star \equiv \min_\Lambda R_p.$$

In this way, we obtain on the class of Bravais lattices that the minimum value of $\mathcal{A}$ at which a competition instability occurs is given by

(4.15)
$$\mathcal{A}_{\mathrm{opt}} = \frac{1}{\sqrt{\nu\mu}} \left(S_{\mathrm{opt}} + \nu \left[\chi(S_{\mathrm{opt}}) + 2\pi S_{\mathrm{opt}} R_p^\star \right] \right), \qquad \frac{1}{\nu} + \chi'(S_{\mathrm{opt}}) = -2\pi \mathcal{K}_{gs}^\star.$$

We emphasize that this result for $\mathcal{A}_{\mathrm{opt}}$ is accurate to all orders in ν. To obtain a two-term asymptotic result $\mathcal{A}_{\mathrm{opt},2}$

for $\mathcal{A}_{\mathrm{opt}}$ in powers of ν when $D = D_0/\nu \gg 1$, we proceed as in [**10**]. For $D \gg 1$, we have that

$$(4.16) \qquad \mathcal{K}_{gs}^\star = \mathcal{K}_{gs0}^\star + \mathcal{O}(\nu), \qquad \mathcal{K}_{gs0} \equiv \max_\Lambda R_{b0}^\star, \qquad R_{b0}^\star \equiv \min_{\boldsymbol{k} \in \Omega_B/(2\pi)} R_{b0}(\boldsymbol{k}),$$

where $R_{b0}(\boldsymbol{k})$ is the regular part of the Bloch Green's function for the Laplacian defined by (3.17), and given explicitly in (3.18). In addition, for $D \gg 1$, we have from (4.4) that $R_p = D|\Omega|^{-1} + R_{p0} + \mathcal{O}(D^{-1})$, where R_{p0} is the regular part of the periodic source-neutral Green's function of (3.8). In this way, for $D = D_0/\nu \gg 1$, (4.15) reduces to

$$(4.17) \quad \mathcal{A}_{\mathrm{opt}} \sim \frac{1}{\sqrt{\nu\mu}} \left[(1+\mu)S_{\mathrm{opt}} + 2\pi\nu S_{\mathrm{opt}} \left(\min_\Lambda R_{p0} \right) + \nu\chi(S_{\mathrm{opt}}) + \mathcal{O}(\nu^2) \right], \qquad \frac{1}{\nu} + \chi'(S_{\mathrm{opt}}) = -2\pi\mathcal{K}_{gs0}^\star + \mathcal{O}(\nu).$$

To obtain an explicit two-term result for $\mathcal{A}_{\mathrm{opt}}$, we use $\chi(S) \sim b/S + \chi_1 S + \cdots$ for $S \ll 1$, as given in (3.4), to obtain from the second equation in (4.17) that

$$S_{\mathrm{opt}} \sim \sqrt{b\nu} \left[1 - \frac{\nu}{2} \left(\chi_1 + 2\pi\mathcal{K}_{gs0}^\star \right) + \mathcal{O}(\nu^2) \right].$$

Upon substituting this expression, together with $\chi'(S) \sim -b/S^2 + \chi_1$, into the first equation of (4.17) we obtain, after some algebra, that

$$(4.18) \qquad \mathcal{A}_{\mathrm{opt}} = \mathcal{A}_{\mathrm{opt},2} + \mathcal{O}(\nu^2), \qquad \mathcal{A}_{\mathrm{opt},2} \equiv \sqrt{\frac{b}{\mu}} \left[2 + \mu + \nu \left(\chi_1 (1 - \mu/2) + 2\pi \min_\Lambda R_{p0} - \mu\pi\mathcal{K}_{gs0}^\star \right) \right],$$

where $\mu \equiv 2\pi D_0/|\Omega|$. This two-term result agrees with that in Principal Result 5.1 of [**10**].

The numerical results of [**10**] showed that $\mathcal{K}_{gs0}^\star$ is attained at a regular hexagonal lattice. In addition, from Theorem 2 of [**4**], $\min_\Lambda R_{p0}$ is also attained at a regular hexagonal lattice. Therefore, from (4.18), the two-term expansion for $\mathcal{A}$ is optimized for a regular hexagonal lattice. On a regular hexagonal lattice, in §5.2 we will compare results from the two-term expansion $\mathcal{A}_{\mathrm{opt},2}$ from (4.18) with the more accurate result $\mathcal{A}_{\mathrm{opt}}$, as obtained by solving the nonlinear algebraic system (4.15), that accounts for all powers in ν. To solve (4.15), we first must obtain analytical results for $R_b(\boldsymbol{k})$ and for R_p, associated with the reduced-wave operator, on an arbitrary lattice Λ.

5 Numerical Computation of the Competition Stability Threshold for the GS model

In this section we compute numerical results for the optimal competition stability threshold for the GS model from (4.15). To do so, we first must extend the analysis of [**3**] and [**10**] to derive an explicit formula for the regular part $R_b(\boldsymbol{k})$ of the Bloch Green's function for the reduced wave-operator, as defined by (2.5). This reduced-wave Green's function was not considered in [**10**].

5.1 Numerical Computation of the Bloch Green's function for the Reduced-Wave Operator

We seek a rapidly converging expansion for the Bloch Green's function for the reduced-wave operator on all of $\mathbb{R}^2$ that satisfies

$$(5.1) \qquad \Delta G_b(\mathbf{x}) - \frac{1}{D} G_b(\mathbf{x}) = -\delta(\mathbf{x}); \qquad G_b(\mathbf{x} + \boldsymbol{l}) = e^{-i\boldsymbol{k}\cdot\boldsymbol{l}} G_b(\mathbf{x}), \qquad \boldsymbol{l} \in \Lambda,$$

where $\boldsymbol{k}/(2\pi) \in \Omega_B$. The regular part $R_b(\boldsymbol{k})$ of this Bloch Green's function is defined by

$$(5.2) \qquad R_b(\boldsymbol{k}) \equiv \lim_{\mathbf{x}\to\mathbf{0}} \left(G_b(\mathbf{x}) + \frac{1}{2\pi} \log |\mathbf{x}| \right).$$

To derive a computationally tractable expression for $R_b(\boldsymbol{k})$ we will follow closely the methodology of [**3**].

We construct the solution to (5.1) as the sum of free-space Green's functions

$$(5.3) \qquad G_b(\mathbf{x}) = \sum_{\boldsymbol{l} \in \Lambda} G_{\text{free}}(\mathbf{x} + \boldsymbol{l}) \, e^{i \boldsymbol{k} \cdot \boldsymbol{l}} \,,$$

which guarantees that the quasi-periodicity condition in (5.1) is satisfied. That is, if $G_b(\mathbf{x}) = \sum_{\boldsymbol{l} \in \Lambda} G_{\text{free}}(\mathbf{x} + \boldsymbol{l}) \, e^{i \boldsymbol{k} \cdot \boldsymbol{l}}$, then, upon choosing any $\boldsymbol{l}^\star \in \Lambda$, we have $G_b(\mathbf{x} + \boldsymbol{l}^\star) = e^{-i \boldsymbol{k} \cdot \boldsymbol{l}^\star} \, G_b(\mathbf{x})$. To show this, we use $\boldsymbol{l}^\star + \boldsymbol{l} \in \Lambda$ and calculate

$$G_b(\mathbf{x} + \boldsymbol{l}^\star) = \sum_{\boldsymbol{l} \in \Lambda} G_{\text{free}}(\mathbf{x} + \boldsymbol{l}^\star + \boldsymbol{l}) \, e^{i \boldsymbol{k} \cdot \boldsymbol{l}} = \sum_{\boldsymbol{l} \in \Lambda} G_{\text{free}}(\mathbf{x} + \boldsymbol{l}^\star + \boldsymbol{l}) \, e^{i \boldsymbol{k} \cdot (\boldsymbol{l}^\star + \boldsymbol{l})} \, e^{-i \boldsymbol{k} \cdot \boldsymbol{l}^\star} = e^{-i \boldsymbol{k} \cdot \boldsymbol{l}^\star} \, G_b(\mathbf{x}) \,.$$

To analyze (5.3) we use the Poisson summation formula with converts a sum over Λ to a sum over the reciprocal lattice $\Lambda^\star$ of (2.2). In the notation of [**3**], we have (see Proposition 2.1 of [**3**])

$$(5.4) \qquad \sum_{\boldsymbol{l} \in \Lambda} f(\mathbf{x} + \boldsymbol{l}) \, e^{i \boldsymbol{k} \cdot \boldsymbol{l}} = \frac{1}{|\Omega|} \sum_{\boldsymbol{d} \in \Lambda^\star} \hat{f}(2\pi \boldsymbol{d} - \boldsymbol{k}) \, e^{i \mathbf{x} \cdot (2\pi \boldsymbol{d} - \boldsymbol{k})} \,, \quad \mathbf{x}, \boldsymbol{k} \in \mathbb{R}^2 \,.$$

Here $|\Omega|$ is the area of the primitive cell of the lattice, and $\hat{f}$ is the Fourier transform of f, defined in $\mathbb{R}^2$ by

$$(5.5) \qquad \hat{f}(\boldsymbol{p}) = \int_{\mathbb{R}^2} f(\mathbf{x}) \, e^{-i \mathbf{x} \cdot \boldsymbol{p}} \, d\mathbf{x} \,, \qquad f(\mathbf{x}) = \frac{1}{4\pi^2} \int_{\mathbb{R}^2} \hat{f}(\boldsymbol{p}) \, e^{i \boldsymbol{p} \cdot \mathbf{x}} \, d\boldsymbol{p} \,.$$

By applying (5.4) to (5.3), it follows that the sum over the reciprocal lattice consists of free-space Green's functions in the Fourier domain, and we will split each Green's function in the Fourier domain into two parts in order to obtain rapidly converging infinite series. The free space Green's function satisfies $\Delta G_{\text{free}} - D^{-1} G_{\text{free}} = -\delta(\mathbf{x})$. By taking Fourier transforms of this equation, we get that $\hat{G}_{\text{free}}(\boldsymbol{p}) = \hat{G}_{\text{free}}(|\boldsymbol{p}|)$, where

$$(5.6) \qquad \hat{G}_{\text{free}}(\rho) = \frac{1}{\rho^2 + \frac{1}{D}} \,, \qquad \rho = |\boldsymbol{p}| \,.$$

In this way, and since $|\Omega| = 1$, we calculate the right-hand side of the Poisson summation formula (5.4) as

$$(5.7) \qquad \frac{1}{|\Omega|} \sum_{\boldsymbol{d} \in \Lambda^\star} \hat{G}_{\text{free}}(2\pi \boldsymbol{d} - \boldsymbol{k}) \, e^{i \mathbf{x} \cdot (2\pi \boldsymbol{d} - \boldsymbol{k})} = \sum_{\boldsymbol{d} \in \Lambda^\star} \frac{e^{i \mathbf{x} \cdot (2\pi \boldsymbol{d} - \boldsymbol{k})}}{|2\pi \boldsymbol{d} - \boldsymbol{k}|^2 + \frac{1}{D}} \,.$$

To obtain a rapidly converging series expansion, we introduce the decomposition

$$(5.8) \qquad \hat{G}_{\text{free}}(2\pi \boldsymbol{d} - \boldsymbol{k}) = \alpha(2\pi \boldsymbol{d} - \boldsymbol{k}, \eta) \, \hat{G}_{\text{free}}(2\pi \boldsymbol{d} - \boldsymbol{k}) + \left(1 - \alpha(2\pi \boldsymbol{d} - \boldsymbol{k}, \eta) \right) \hat{G}_{\text{free}}(2\pi \boldsymbol{d} - \boldsymbol{k}) \,,$$

where the function $\alpha(2\pi \boldsymbol{d} - \boldsymbol{k}, \eta)$ is chosen as

$$(5.9) \qquad \alpha(2\pi \boldsymbol{d} - \boldsymbol{k}, \eta) = \exp\left(-\frac{|2\pi \boldsymbol{d} - \boldsymbol{k}|^2 + \frac{1}{D}}{\eta^2} \right) \,.$$

Here $\eta > 0$ is a cutoff parameter to be specified below. With this choice for α, it is readily verified that

$$\lim_{\eta \to 0} \alpha(2\pi \boldsymbol{d} - \boldsymbol{k}, \eta) = 0 \,; \qquad \lim_{\eta \to \infty} \alpha(2\pi \boldsymbol{d} - \boldsymbol{k}, \eta) = 1 \,; \qquad \frac{\partial \alpha}{\partial \eta} > 0 \,, \quad \text{since } \alpha > 0 \,, \ \eta > 0 \,,$$

which shows that $0 < \alpha < 1$ when $0 < \eta < \infty$.

With this choice for α, the sum over $\boldsymbol{d} \in \Lambda^\star$ of the first set of terms in (5.8) converges absolutely. We will apply the inverse transform (5.5) to the second set of terms in (5.8) after first writing $(1 - \alpha) \, \hat{G}_{\text{free}}$ as an integral. In this way, since $0 < \alpha < 1$, the choice of η determines the portion of the Green's function that is determined from the sum of terms in the reciprocal lattice $\Lambda^\star$ and the portion that is determined from the sum of terms in the lattice Λ.

With the expressions (5.9) for α and (5.6) for $\hat{G}_{\text{free}}$, we get

$$(5.10) \qquad \alpha(2\pi \boldsymbol{d} - \boldsymbol{k}, \eta) \, \hat{G}_{\text{free}}(2\pi \boldsymbol{d} - \boldsymbol{k}) \, e^{i \mathbf{x} \cdot (2\pi \boldsymbol{d} - \boldsymbol{k})} = \exp\left(-\frac{|2\pi \boldsymbol{d} - \boldsymbol{k}|^2 + \frac{1}{D}}{\eta^2} \right) \frac{e^{i \mathbf{x} \cdot (2\pi \boldsymbol{d} - \boldsymbol{k})}}{|2\pi \boldsymbol{d} - \boldsymbol{k}|^2 + \frac{1}{D}} \,.$$

Thus, for all $\boldsymbol{k}$, the sum of these terms over $\boldsymbol{d} \in \Lambda^\star$ will converge absolutely. Following [3], we then define

$$(5.11) \qquad G_{\text{fourier}}(\mathbf{x}) = \sum_{\boldsymbol{d} \in \Lambda^\star} \exp\left(-\frac{|2\pi\boldsymbol{d} - \boldsymbol{k}|^2 + \frac{1}{D}}{\eta^2}\right) \frac{e^{i\mathbf{x}\cdot(2\pi\boldsymbol{d} - \boldsymbol{k})}}{|2\pi\boldsymbol{d} - \boldsymbol{k}|^2 + \frac{1}{D}} .$$

For the $(1 - \alpha)\,\hat{G}_{\text{free}}$ term in (5.8), we define ρ by $\rho \equiv |2\pi\boldsymbol{d} - \boldsymbol{k}|$, so that from (5.9) and (5.6), we get

$$(5.12) \qquad (1 - \alpha(2\pi\boldsymbol{d} - \boldsymbol{k}, \eta))\,\hat{G}_{\text{free}}(2\pi\boldsymbol{d} - \boldsymbol{k}) = \frac{1}{\rho^2 + \frac{1}{D}}\left(1 - \exp\left(-\frac{\rho^2 + \frac{1}{D}}{\eta^2}\right)\right) .$$

Since $\int e^{-\left(\rho^2 + \frac{1}{D}\right)e^{-2s} - 2s}\,ds = e^{-\left(\rho^2 + \frac{1}{D}\right)e^{-2s}} / \left[2\left(\rho^2 + \frac{1}{D}\right)\right]$, we calculate

$$(5.13) \qquad 2\int_{\log\eta}^{\infty} e^{-\left(\rho^2 + \frac{1}{D}\right)e^{-2s} - 2s}\,ds = \left.\frac{e^{-\left(\rho^2 + \frac{1}{D}\right)e^{-2s}}}{\rho^2 + \frac{1}{D}}\right|_{s=\log\eta}^{s=\infty} = \frac{1}{\rho^2 + \frac{1}{D}}\left(1 - e^{-\frac{\rho^2 + \frac{1}{D}}{\eta^2}}\right) ,$$

so that from (5.12) and (5.13), we obtain

$$(5.14) \qquad (1 - \alpha)\,\hat{G}_{\text{free}} = \int_{\log\eta}^{\infty} 2\,e^{-\left(\rho^2 + \frac{1}{D}\right)e^{-2s} - 2s}\,ds .$$

To take the inverse Fourier transform of (5.14), we recall that the inverse Fourier transform of a radially symmetric function is the inverse Hankel transform of order zero (cf. [23]), so that $f(r) = (2\pi)^{-1}\int_0^\infty \hat{f}(\rho)\,J_0(\rho r)\,\rho\,d\rho$. Upon using the well-known inverse Hankel transform (cf. [23])

$$\int_0^\infty e^{-\rho^2\,e^{-2s}}\,\rho\,J_0(\rho r)\,d\rho = \frac{1}{2}\,e^{2s - r^2\,e^{2s}/4} ,$$

we calculate the inverse Fourier transform of (5.14) as

$$\frac{1}{2\pi}\int_0^\infty\int_{\log\eta}^{\infty} 2\,e^{-\left(\rho^2 + \frac{1}{D}\right)e^{-2s} - 2s}\,\rho\,J_0(\rho r)\,ds\,d\rho = \frac{1}{\pi}\int_{\log\eta}^{\infty} e^{-2s - e^{-2s}/D}\left(\int_0^\infty e^{-\rho^2 e^{-2s}}\,\rho\,J_0(\rho r)\,d\rho\right) ds$$

$$= \frac{1}{2\pi}\int_{\log\eta}^{\infty} e^{-2s - e^{-2s}/D}\,e^{2s - \frac{r^2}{4}\,e^{2s}}\,ds = \frac{1}{2\pi}\int_{\log\eta}^{\infty} e^{-\left(\frac{r^2}{4}\,e^{2s} + \frac{1}{D}\,e^{-2s}\right)}\,ds .$$

In the notation of [3], we then define $F_{\text{sing}}(|\mathbf{x}|)$ as

$$(5.15) \qquad F_{\text{sing}}(|\mathbf{x}|) \equiv \frac{1}{2\pi}\int_{\log\eta}^{\infty} e^{-\left(\frac{|\mathbf{x}|^2}{4}\,e^{2s} + \frac{1}{D}\,e^{-2s}\right)}\,ds ,$$

so that by the Poisson summation formula (5.4), we have

$$(5.16) \qquad G_{\text{spatial}}(\mathbf{x}) \equiv F_{\text{sing}}(|\mathbf{x}|) + \sum_{\substack{\boldsymbol{l} \in \Lambda \\ \boldsymbol{l} \neq 0}} e^{i\boldsymbol{k}\cdot\boldsymbol{l}}\,F_{\text{sing}}(|\mathbf{x} + \boldsymbol{l}|) .$$

In this way, we write the Bloch Green's function for the reduced-wave operator in the spatial domain as the sum of (5.11) and (5.16)

$$(5.17) \qquad G_b(\mathbf{x}) = \sum_{\boldsymbol{d} \in \Lambda^\star} \frac{e^{-\frac{|2\pi\boldsymbol{d} - \boldsymbol{k}|^2 + \frac{1}{D}}{\eta^2}}\,e^{i\mathbf{x}\cdot(2\pi\boldsymbol{d} - \boldsymbol{k})}}{|2\pi\boldsymbol{d} - \boldsymbol{k}|^2 + \frac{1}{D}} + F_{\text{sing}}(|\mathbf{x}|) + \sum_{\substack{\boldsymbol{l} \in \Lambda \\ \boldsymbol{l} \neq 0}} e^{i\boldsymbol{k}\cdot\boldsymbol{l}}\,F_{\text{sing}}(|\mathbf{x} + \boldsymbol{l}|) ,$$

where $F_{\text{sing}}(|\mathbf{x}|)$ is defined in (5.15). From (5.11) and (5.16), it readily follows that $G_{\text{fourier}}(\mathbf{x}) \to 0$ as $\eta \to 0$, while $G_{\text{spatial}}(\mathbf{x}) \to 0$ as $\eta \to \infty$.

To derive an expression for $R_b(\boldsymbol{k})$, we first must calculate the behaviour of $G_b(\mathbf{x})$ as $\mathbf{x} \to 0$. From (5.11), we have

$$(5.18) \qquad G_{\text{fourier}}(0) = \sum_{\boldsymbol{d} \in \Lambda^\star} \exp\left(-\frac{|2\pi\boldsymbol{d} - \boldsymbol{k}|^2 + \frac{1}{D}}{\eta^2}\right) \frac{1}{|2\pi\boldsymbol{d} - \boldsymbol{k}|^2 + \frac{1}{D}},$$

which is finite for all $|2\pi\boldsymbol{d} - \boldsymbol{k}|$ and $0 < \eta < \infty$. For the last set of terms in (5.17), we can take the limit $\mathbf{x} \to 0$ to get

$$\left| \sum_{\substack{\boldsymbol{l} \in \Lambda \\ \boldsymbol{l} \neq 0}} e^{i\boldsymbol{k}\cdot\boldsymbol{l}} F_{\text{sing}}(|\boldsymbol{l}|) \right| < \infty \,.$$

In contrast, $F_{\text{sing}}(r)$ with $r = |\mathbf{x}|$ is singular at $\mathbf{x} = 0$. The integrand in (5.15) has a maximum at the point $s = s_m$, where the function $\xi \equiv -r^2 e^{2s}/4 - e^{-2s}/D$ has a maximum. After calculating this maximum point, labelled by s_m, we introduce a change of variables

$$s = s_m + t/2 \,, \qquad s_m = -\frac{1}{2}\log r - \frac{1}{4}\log\left(D/4\right) \,.$$

In terms of t, we readily calculate that $\xi = -(r/\sqrt{D})\cosh t$, so that $F_{\text{sing}}(r)$ in (5.15) becomes

$$(5.19) \qquad F_{\text{sing}}(r) = \frac{1}{4\pi}\int_\beta^\infty e^{-(r/\sqrt{D})\cosh t}\,dt\,, \qquad \beta \equiv \log\left(\frac{\eta^2 r\sqrt{D}}{2}\right)\,,$$

with the maximum of the integrand occurring at $t = 0$. It is then convenient to decompose $F_{\text{sing}}(r)$ as follows:

Lemma 5.1 *The integral* $F_{\text{sing}}(r)$ *defined in (5.19) can be written as*

$$(5.20\,a) \qquad F_{\text{sing}}(r) = \begin{cases} \frac{1}{2\pi}K_0\left(\frac{r}{\sqrt{D}}\right) - \frac{1}{4\pi}\left[E_1\left(\frac{r}{\sqrt{D}}\cosh\beta\right) + J\right]\,, & \text{for } \frac{\eta^2 r\sqrt{D}}{2} \leq 1\,, \\ \frac{1}{4\pi}\left[E_1\left(\frac{r}{\sqrt{D}}\cosh\beta\right) + J\right]\,, & \text{for } \frac{\eta^2 r\sqrt{D}}{2} \geq 1\,, \end{cases}$$

where $E_1(z) \equiv \int_z^\infty t^{-1}e^{-t}\,dt$ *is the exponential integral,* $\beta \equiv \log\left(\frac{\eta^2 r\sqrt{D}}{2}\right)$, *and the integral* J *is defined by*

$$(5.20\,b) \qquad J \equiv \int_{(r/\sqrt{D})\cosh\beta}^\infty \frac{e^{-t}}{t}\left(\frac{1}{\sqrt{1 - r^2/(Dt^2)}} - 1\right)dt\,.$$

The asymptotic behaviour of $F_{\text{sing}}(r)$ *as* $r \to 0$ *is*

$$(5.21) \qquad F_{\text{sing}}(r) \sim -\frac{1}{2\pi}\log r + \frac{1}{2\pi}\left[\log\left(2\sqrt{D}\right) - \gamma\right] - \frac{1}{4\pi}E_1\left(1/\eta^2 D\right)\,,$$

where $\gamma = 0.57721\ldots$ *is Euler's constant.*

<u>Proof:</u> We first assume $\eta^2 r\sqrt{D}/2 \leq 1$, so that $\beta \leq 0$. Since the integrand in (5.19) is even in t, we decompose it as

$$F_{\text{sing}}(r) = \frac{1}{2\pi}\int_0^\infty e^{-(r/\sqrt{D})\cosh t}\,dt - \frac{1}{4\pi}\int_{-\infty}^\beta e^{-(r/\sqrt{D})\cosh t}\,dt\,.$$

In the first integral we let $w = \cosh t$ and use $K_0(z) = \int_1^\infty (w^2 - 1)^{-1/2} e^{-zw}\,dw$, where $K_0(z)$ for $z > 0$ is the modified Bessel function of the second kind of order zero. In the second integral, we let $w = \cosh t$ for $t \leq 0$. This yields

$$(5.22) \qquad F_{\text{sing}}(r) = \frac{1}{2\pi}K_0\left(r/\sqrt{D}\right) - \frac{1}{4\pi}\int_{\cosh\beta}^\infty \frac{e^{-(r/\sqrt{D})w}}{\sqrt{w^2 - 1}}\,dw\,.$$

We then add and subtract a term for the integral in (5.22) to get

$$
(5.23) \qquad F_{\text{sing}}(r) = \frac{1}{2\pi} K_0 \left(r/\sqrt{D} \right) - \frac{1}{4\pi} \left[\int_{\cosh \beta}^{\infty} \frac{e^{-(r/\sqrt{D})w}}{w} + \int_{\cosh \beta}^{\infty} \left(\frac{e^{-(r/\sqrt{D})w}}{\sqrt{w^2-1}} - \frac{e^{-(r/\sqrt{D})w}}{w} \right) dw \right].
$$

Then, setting $t = rw/\sqrt{D}$ in (5.23), we readily obtain the first equation in (5.20 a). Next, we calculate that

$$
(5.24) \qquad \frac{r}{\sqrt{D}} \cosh \beta = \frac{1}{\eta^2 D} \left[1 + \frac{\left(\eta^2 D \right)^2}{4} \left(\frac{r}{\sqrt{D}} \right)^2 \right].
$$

Therefore, as $r \to 0$, we have from (5.20 b) and (5.24) that

$$
(5.25) \qquad J \sim \frac{r^2}{2D} \int_{1/(\eta^2 D)}^{\infty} \frac{e^{-t}}{t^3} \, dt = \mathcal{O}(r^2).
$$

Since $J \to 0$ and $\left(r/\sqrt{D} \right) \cosh \beta \to 1/(\eta^2 D)$ as $r \to 0$, we use the well-known asymptotics $K_0(z) \sim -\log z + \log 2 - \gamma + o(1)$ (cf. [1]), to readily obtain that the first line in (5.20 a) yields (5.21) as $r \to 0$.

To establish the second line in (5.20 a) we begin with (5.19) for $\beta \geq 0$, and let $w = \cosh t$. In terms of w, we write

$$
(5.26) \qquad F_{\text{sing}}(r) = \frac{1}{4\pi} \left[\int_{\cosh \beta}^{\infty} \frac{e^{-(r/\sqrt{D})w}}{w} + \int_{\cosh \beta}^{\infty} \left(\frac{e^{-(r/\sqrt{D})w}}{\sqrt{w^2-1}} - \frac{e^{-(r/\sqrt{D})w}}{w} \right) dw \right].
$$

Upon setting $t = (r/\sqrt{D})w$ in the two integrals in (5.26), we readily obtain the second line in (5.20 a). ∎

The result in (5.20) expresses $F_{\text{sing}}(r)$ in terms of standard special functions together with an integral J, depending on the two parameters $r/\sqrt{D}$ and $\eta^2 D$, that must be calculated numerically. For $\eta^2 D = \mathcal{O}(1)$, one key advantage for computing J numerically, as is easily observed from (5.20 a) and (5.24), is that $J = o(1)$ when either $r/\sqrt{D}$ is small or large. Then, upon substituting (5.21) into (5.17), and letting $\mathbf{x} \to 0$, we can identify $R_b(\mathbf{k})$ in (5.2) as

(5.27)
$$
R_b(\boldsymbol{k}) = \frac{1}{2\pi} \left(\log \left(2\sqrt{D} \right) - \gamma - \frac{E_1 \left[1/(\eta^2 D) \right]}{2} \right) + \sum_{\boldsymbol{d} \in \Lambda^\star} \exp \left(-\frac{|2\pi \boldsymbol{d} - \boldsymbol{k}|^2 + \frac{1}{D}}{\eta^2} \right) \frac{1}{|2\pi \boldsymbol{d} - \boldsymbol{k}|^2 + \frac{1}{D}} + \sum_{\substack{\boldsymbol{l} \in \Lambda \\ \boldsymbol{l} \neq \boldsymbol{0}}} e^{i \boldsymbol{k} \cdot \boldsymbol{l}} F_{\text{sing}}(|\boldsymbol{l}|).
$$

Finally, to obtain R_p in (4.4), as needed in (4.10), we simply set $\boldsymbol{k} = \boldsymbol{0}$ in (5.27) to identify $R_p = R_b(\boldsymbol{0})$.

5.2 Numerical Results for the Stability Threshold

In this subsection we calculate the optimal competition stability threshold for the GS model from (4.15). As such, we must compute $R_b(\boldsymbol{k})$ and $R_p \equiv R_b(\boldsymbol{0})$ from (5.27). To compute these quantities we introduce subsets $\bar{\Lambda}$ and $\bar{\Lambda}^\star$ of the direct and reciprocal lattices Λ and $\Lambda^\star$, respectively, defined by

$$
(5.28) \qquad \bar{\Lambda} \equiv \left\{ n_1 \boldsymbol{l}_1 + n_2 \boldsymbol{l}_2 \, \big| \, -M_1 < n_1, n_2 < M_1 \right\}, \quad \bar{\Lambda}^\star \equiv \left\{ n_1 \boldsymbol{d}_1 + n_2 \boldsymbol{d}_2 \, \big| \, -M_2 < n_1, n_2 < M_2 \right\}, \quad n_1, n_2 \in \mathbb{Z}.
$$

In our computations of $R_b(\boldsymbol{k})$ we set $\eta = 3$, $M_1 = 3$, and $M_2 = 5$. Using larger values of M_1 or M_2 or using other values of η between 2 and 4 had a negligible effect on our computed values of $R_b(\boldsymbol{k})$ and $R_p = R_b(\boldsymbol{0})$. In order to compute $R_b^\star \equiv \min_{\boldsymbol{k} \in \Omega_B/(2\pi)} R_b(\boldsymbol{k})$, we first use a coarse grid to find an approximate location in $\boldsymbol{k}$-space of the minimum of $R_b(\boldsymbol{k})$. After establishing by a coarse discretization that the minimum arises near a vertex of the reciprocal lattice, we then sample more finely near this vertex. The finest mesh has a resolution of $\pi/100$. To determine the value of
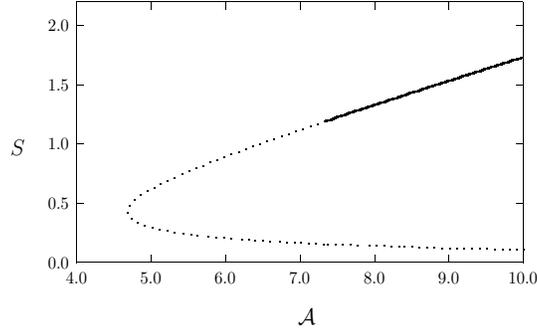
Figure 6. Plot of the saddle-node bifurcation diagram S versus $\mathcal{A}$, obtained from (5.29), for the GS model for a periodic pattern of spots on a regular hexagonal lattice with $|\Omega| = 1$, $D_0 = 1$, and $\varepsilon = 0.02$. The heavy solid and dotted branches are linearly stable and linearly unstable, respectively, to competition instabilities. To leading order in ν, the zero eigenvalue crossing corresponding to the competition instability threshold occurs at $\mathcal{A}_0 = (2 + \mu) \sqrt{b/\mu} \approx 7.34$.

$R_b^\star$ we interpolate a paraboloid through the approximate minimum and the four neighbouring points and evaluate the minimum of the paraboloid.

As shown in §4, the bifurcation diagram of S versus A for a one-spot pattern is given by

$$(5.29) \qquad A = \varepsilon \sqrt{\frac{2\pi}{|\Omega|}} \mathcal{A}, \qquad \mathcal{A} = \frac{1}{\sqrt{\nu\mu}} \left(S + \nu \left[\chi(S) + 2\pi S R_p \right] \right),$$

where $\mu = 2\pi D_0/|\Omega|$ and $D = D_0/\nu$. Here R_p is computed from (5.27) with $R_p = R_b(\mathbf{0})$. In Fig. 6 we plot the bifurcation diagram of S versus $\mathcal{A}$ for a regular hexagonal lattice with $|\Omega| = 1$ when $\varepsilon = 0.02$ and $D_0 = 1$, so that $\nu = 0.256$ and $D = 3.912$. The bifurcation diagram is seen to have a fold-point structure. The leading-order-in-ν result for the competition instability threshold is $\mathcal{A}_0 \equiv \frac{(2+\mu)\sqrt{b}}{\sqrt{\mu}} \approx 7.34$, and is indicated in Fig. 6. Only the heavy solid portion of the solution branch in Fig. 6 is stable to competition instabilities (cf. [**10**]).

Next, on a regular hexagonal lattice with $|\Omega| = 1$ and for a range of values of ν, we compare the stability thresholds from the nonlinear algebraic system (4.15), and from the two-term result (4.18). For the formulation (4.15), which is accurate to all orders in ν, we choose $D_0 = 1$ and use $D = D_0/\nu = \nu^{-1}$ in computing $R_b^\star$ and R_p from (5.27) on the hexagonal lattice. Newton's method is then used to compute $\mathcal{A}_{\mathrm{opt}}$ from (4.15). In contrast, on a regular hexagonal lattice, and with $D = D_0/\nu = \nu^{-1} \gg 1$ and $\mu = 2\pi D_0/|\Omega| = 2\pi$, the two-term expansion $\mathcal{A}_{\mathrm{opt},2}$ from (4.18) is

$$(5.30\,a) \qquad\qquad\qquad \mathcal{A}_{\mathrm{opt},2} \sim \mathcal{A}_0 + \nu \mathcal{A}_1 + \cdots,$$

$$(5.30\,b) \qquad \mathcal{A}_0 \equiv \frac{(2+\mu)\sqrt{b}}{\sqrt{\mu}} \approx 7.34, \qquad \mathcal{A}_1 = \sqrt{\frac{b}{\mu}} \left(2\pi R_{p0} - \mu\pi R_{b0}^\star + \chi_1 \left(1 - \frac{\mu}{2} \right) \right) \approx 0.1764,$$

where we have used the values $R_{b0}^\star \equiv \min_{\mathbf{k} \in \Omega_B/(2\pi)} R_{b0}(\mathbf{k}) \approx -0.079124$ and $R_{p0} \approx -0.21027$.

In Fig. 7 we compare the numerically computed $\mathcal{A}_{\mathrm{opt}}$ from (4.15) with the two-term result (5.30) for a range of ν. The left panel of Fig. 7 is for $0 < \nu < 0.44$, which corresponds to $0 < \varepsilon < 0.10$. At $\nu = 0.34$, for which $\epsilon \approx 0.05$, the difference between $\mathcal{A}_{\mathrm{opt}}$ and the two-term expansion $\mathcal{A}_{\mathrm{opt},2}$ is about 8.3%. At $\nu = 0.22$, corresponding to $\epsilon \approx 0.01$, this difference shrinks to about 2.8%. Thus, at only moderately small ε such as $\varepsilon = 0.05$, the formulation (4.15) provides a significantly more accurate determination of the competition stability threshold than does the two-term result (5.30). For much smaller values of $\varepsilon = e^{-1/\nu}$, the right panel of Fig. 7 shows that $\mathcal{A}_{\mathrm{opt},2} \to \mathcal{A}_{\mathrm{opt}}$ as $\nu \to 0$.

Finally, to examine how the competition stability threshold depends on the lattice, we consider the simple class of

$$0 < \varepsilon < 0.10 \qquad\qquad\qquad\qquad 0 < \varepsilon < 0.000045$$
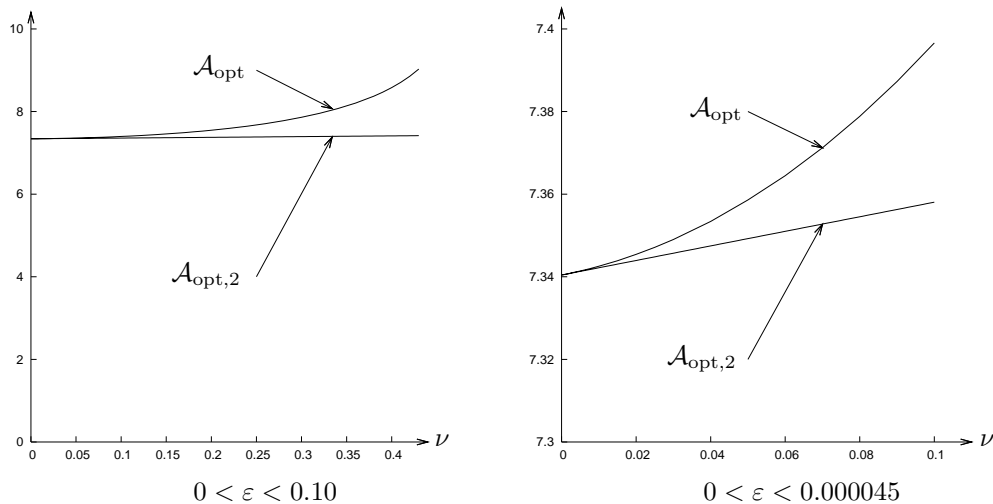
Figure 7. Comparison of the two-term result $\mathcal{A}_{\mathrm{opt},2}$, from (5.30), and the hybrid asymptotic-numerical result $\mathcal{A}_{\mathrm{opt}}$, from (4.15), versus $\nu = -1/\log\varepsilon$. These results predict the optimal competition stability threshold for a periodic pattern of spots for the GS model on a regular hexagonal lattice with $|\Omega| = 1$ and $D = 1/\nu$.

lattices Λ for which $|\boldsymbol{l}_1| = |\boldsymbol{l}_2|$, given by $\boldsymbol{l}_1 = (1/\sqrt{\sin(\theta)}, 0)$ and $\boldsymbol{l}_2 = (\cos(\theta)/\sqrt{\sin(\theta)}, \sqrt{\sin(\theta)})$, where the parameter θ is the angle with respect to the horizontal axis. We fix $D_0 = 1$, $\varepsilon = 0.05$, so that $\nu \approx 0.334$ and $D = 1/\nu \approx 2.996$. As θ is varied, we compute the competition stability threshold that is accurate to all orders in ν, which satisfies

$$(5.31) \qquad \mathcal{A} = \frac{1}{\sqrt{\nu\mu}}\left(S + \nu\left[\chi(S) + 2\pi SR_p\right]\right), \qquad \frac{1}{\nu} + \chi'(S) = -2\pi R_b^{\star}.$$

where R_p and $R_b^{\star} = \min_{\boldsymbol{k}\in\Omega_B/(2\pi)} R_b(\boldsymbol{k})$ must be computed at $D = 1/\nu \approx 2.996$ from (5.27) at each lattice angle θ. In terms of the solution $\mathcal{A}$ to (5.31), we define $\mathcal{A}_{\mathrm{num},1} \equiv \left[\mathcal{A} - \mathcal{A}_0\right]/\nu$, where $\mathcal{A}_0 \equiv \frac{(2+\mu)\sqrt{b}}{\sqrt{\mu}} \approx 7.34$. In Fig. 8 we plot $\mathcal{A}_{\mathrm{num},1}$ versus θ and compare it with the correction term $\mathcal{A}_1$ from the two-term asymptotic theory, given by

$$(5.32) \qquad \mathcal{A}_1 = \sqrt{\frac{b}{\mu}}\left(2\pi R_{p0} - \mu\pi R_{b0}^{\star} + \chi_1\left(1 - \frac{\mu}{2}\right)\right), \qquad b \approx 4.93, \qquad \chi_1 \approx 0.0194.$$

Here R_{p0} and $R_{b0}^{\star}$ are computed from (3.9) (see Fig. 3) and (3.18), respectively. This plot shows that the hybrid theory (5.31), based on the regular part of the Bloch Green's function for the reduced-wave operator, also predicts that the optimal stability threshold is attained for a regular hexagonal lattice. The plot also shows that the two-term asymptotic theory is only in fair agreement with results from the more accurate hybrid approach when $\varepsilon = 0.05$.

6 Discussion

The stability threshold associated with periodic patterns of localized spots for two specific two-component RD systems in the limit of an asymptotically large ratio $\mathcal{O}(\varepsilon^{-2})$ of the diffusivities has an asymptotic expansion in powers of the logarithmic gauge $\nu \equiv -1/\log\varepsilon$. In [10] a semi-rigorous analytical method, combining the method of matched asymptotic expansions with a detailed spectral theory, was used to derive a two-term asymptotic expansion for this stability threshold for the Schnakenberg, GS, and Gierer-Meinhardt RD systems. However, as is typical with infinite logarithmic series, the two-term expansion is not expected to provide a very accurate prediction of the stability threshold when ε is only moderately small.

To overcome this difficulty, we formulated and implemented a hybrid asymptotic-numerical method for determining
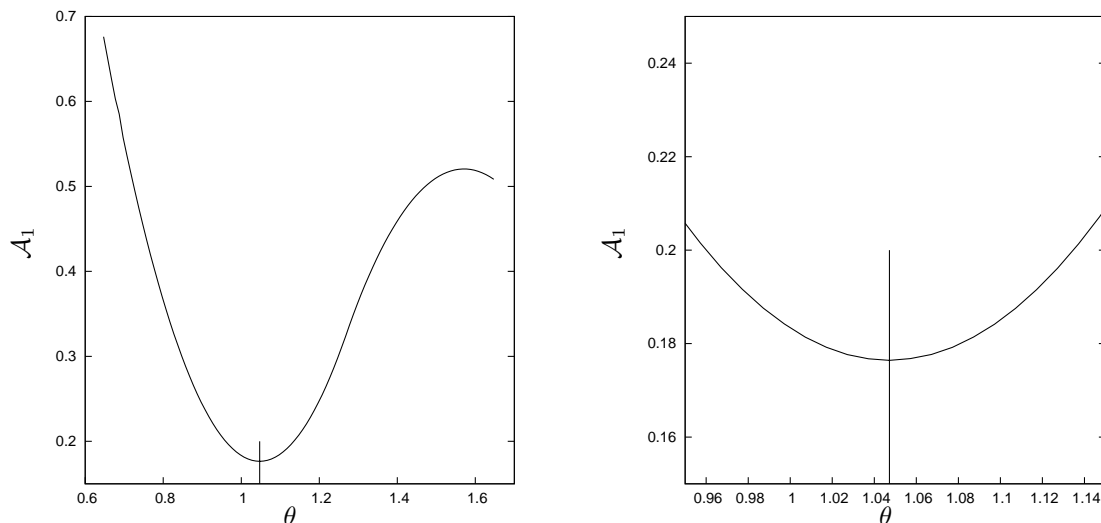
Figure 8. Comparison of competition stability thresholds on the class of Bravais lattices with $|\boldsymbol{l}_1| = |\boldsymbol{l}_2|$, given by $\boldsymbol{l}_1 = (1/\sqrt{\sin(\theta)}, 0)$ and $\boldsymbol{l}_2 = (\cos(\theta)/\sqrt{\sin(\theta)}, \sqrt{\sin(\theta)})$, where the angle θ is a parameter. For $\varepsilon = 0.05$ and $D = -\log(0.05) \approx 2.996$, we compare $\mathcal{A}_{\mathrm{num},1} \equiv [\mathcal{A} - \mathcal{A}_0]/\nu$ from the hybrid theory (5.31) with the coefficient $\mathcal{A}_1$ given in (5.32) from the two-term asymptotic theory. The hybrid theory predicts that the optimal threshold is attained for a regular hexagonal lattice.

an approximation to the stability threshold that is accurate to all orders in ν. Although we have focused our analysis only on the Schnakenberg and GS models, we emphasize that a similar hybrid method can be formulated for many other two-component RD systems. The hybrid formulation consists of a nonlinear algebraic system involving a function associated with the locally radially symmetric spot profile within the fundamental cell of the lattice together with the regular part of this Bloch Green's function for the reduced-wave operator. The nonlinear function associated with the spot profile depends on the specific RD system, and must be computed from a numerical solution to a simple ODE boundary value problem. In contrast, the regular part of the Bloch Green's function, which depends on the Bloch wavevector, is independent of the specific RD system. A key step in our analysis was to derive a rapidly converging infinite series representation for the regular part of this Green's function. Our numerical computations for the Schnakenberg and GS models show, as expected, that there is a rather significant difference, at finite ε, in the prediction of the stability threshold from the two-term and the hybrid theories.

Acknowledgements

References

[1] M. Abramowitz, I. Stegun, *Handbook of mathematical functions*, 9th edition, New York, NY, Dover Publications.

[2] N. Ashcroft, N. D. Mermin, *Solid state physics*, HRW International Relations, CBS Publishing Asia Ltd (1976).

[3] G. Beylkin, C. Kurcz, L. Monzón, *Fast algorithms for Helmholtz Green's functions*, Proc. R. Soc. A, **464**, (2008), pp. 3301-3326.

[4] X. Chen, Y. Oshita, *An application of the modular function in nonlocal variational problems*, Arch. Rational Mech. Anal., **186**(1), (2007), pp. 109-132.

[5] W. Chen, M. J. Ward, *The stability and dynamics of localized spot patterns in the two-dimensional Gray-Scott model*, SIAM J. Appl. Dyn. Sys., **10**(2), (2011), pp. 582–666.

[6] A. Doelman, R. A. Gardner, T. Kaper, *Large stable pulse solutions in reaction-diffusion equations*, Indiana U. Math. Journ., **50**(1), (2001), pp. 443-507.

[7] A. Doelman, R. A. Gardner, T. Kaper, *A stability index analysis of 1-D patterns of the Gray-Scott model*, Memoirs of the AMS **155** (737), (2002).

[8] S. Hormozi, M. J. Ward, *A hybrid asymptotic-numerical method for calculating drag coefficients in 2-D low Reynolds number flow*, to appear, J. Eng. Math., (2014), (30 pages).

[9] D. Iron, M. J. Ward and J. Wei, *The stability of spike solutions to the one-dimensional Gierer-Meinhardt model*, Physica D, **150**(1-2), (2001), pp. 25–62.

[10] D. Iron, J. Rumsey, M. J. Ward and J. Wei, *Logarithmic expansions and the stability of periodic patterns of localized spots for reaction-diffusion systems in* $\mathbb{R}^2$, J. Nonlinear Sci., online first, (2014).

[11] T. Kolokolnikov, M. J. Ward, J. Wei, *Spot self-replication and dynamics for the Schnakenberg Model in a two-dimensional domain*, J. Nonlinear Sci., **19**(1), (2009), pp. 1–56.

[12] T. Kolokolnikov, M. S. Titcombe, M. J. Ward, *Optimizing the fundamental Neumann eigenvalue for the Laplacian in a domain with small traps*, European J. Appl. Math., **16**(2), (2005), pp. 161–200.

[13] I. M. Krichever, *Spectral theory of two-dimensional periodic operators and its applications*, Russian Mathematical Surveys, **44**(2), (1989), pp. 145–225.

[14] M. C. Kropinski, M. J. Ward, J. B. Keller, *A hybrid asymptotic-numerical method for calculating low reynolds number flows past symmetric cylindrical bodies*, SIAM J. Appl. Math., **55**(6), (1995), pp. 1484–1510.

[15] P. Kuchment, *Floquet theory for partial differential equations*, Birkhauser, Basel, 1993.

[16] M. C. Kropinski, A. Lindsay, M. J. Ward, *Asymptotic analysis of localized solutions to some linear and nonlinear biharmonic eigenvalue problems*, Studies in Appl. Math., **126**(4), (2011), 347–408.

[17] C. M. Linton, *Lattice sums for the Helmholtz equation*, SIAM Rev., **52**(4), (2010), pp. 630–674.

[18] A. Moroz, *Quasi-periodic Green's functions of the Helmholz and Laplace equations*, J. Phys. A: Math. Gen., **39**(36), (2006), pp. 11247-11282.

[19] C. Muratov, V. V. Osipov, *Static spike autosolitons in the Gray-Scott model*, J. Phys. A: Math Gen. **33**, (2000), pp. 8893–8916.

[20] C. Muratov, V. V. Osipov, *Spike autosolitons and pattern formation scenarios in the two-dimensional Gray-Scott model*, Eur. Phys. J. B. **22**, (2001), pp. 213–221.

[21] C. Muratov and V. V. Osipov, *Stability of static spike autosolitons in the Gray-Scott model*, SIAM J. Appl. Math., **62**(5), (2002), pp. 1463–1487.

[22] Y. Nishiura, *Far-from equilibrium dynamics, translations of mathematical monographs*, Vol. **209**, AMS Publications, Providence, Rhode Island, (2002).

[23] R. Piessens, "The Hankel Transform", *The transforms and applications handbook: second edition* Editor: Alexander D. Poularikas Boca Raton: CRC Press LLC, 2000.

[24] S. Pillay, M. J. Ward, A. Pierce, T. Kolokolnikov, *An asymptotic analysis of the mean first passage time for narrow escape problems: Part I: two-dimensional domains*, SIAM Multiscale Modeling and Simul., **8**(3), (2010), pp. 803–835.

[25] I. Rozada, S. Ruuth, M. J. Ward, *The stability of localized spot patterns for the Brusselator on the sphere*, SIAM J. Appl. Dyn. Sys., **13**(1), (2014), pp. 564–627.

[26] H. Van der Ploeg, A. Doelman, *Stability of spatially periodic pulse patterns in a class of singularly perturbed reaction-diffusion equations*, Indiana Univ. Math. J., **54**(5), (2005), pp. 1219-1301.

[27] V. K. Vanag, I. R. Epstein, *Localized patterns in reaction-diffusion systems*, Chaos, **17**(3), 037110, (2007).

[28] A. G. Vladimirov, J. M. McSloy, D. S. Skryabin, W. J. Firth, *Two-dimensional clusters of solitary structures in driven optical cavities*, Phys. Rev. E., **65** 046606, (2002)

[29] M. J. Ward, M. C. Kropinski, *Asymptotic methods for PDE problems in fluid mechanics and related systems with strong localized perturbations in two dimensional domains, book chapter in: Asymptotic Methods in Fluid Mechanics: Surveys and Results. CISM International centre for mechanical science,* **523**, (2010), 23–70.

[30] M. J. Ward, W. D. Henshaw, J. Keller, *Summing logarithmic expansions for singularly perturbed eigenvalue problems*, SIAM J. Appl. Math, **53**(3), (1993), pp. 799–828.

[31] M. J. Ward, J. Wei, *Hopf bifurcations and oscillatory instabilities of spike solutions for the one-dimensional Gierer-Meinhardt model*, J. Nonlinear Sci., **13**(2), (2003), pp. 209–264.

[32] J. Wei, *On single interior spike solutions for the Gierer-Meinhardt system: uniqueness and stability estimates*, Europ. J. Appl. Math., **10**(4), (1999), pp. 353-378.

[33] J. Wei, M. Winter, *Spikes for the two-dimensional Gierer-Meinhardt system: the weak coupling case*, J. Nonlinear Sci., **11**(6), (2001), pp. 415–458.

[34] J. Wei, M. Winter, *Existence and stability of multiple spot solutions for the Gray-Scott model in* $\mathbb{R}^2$, Physica D, **176**(3-4), (2003), pp. 147–180.

[35] J. Wei, M. Winter, *Stationary multiple spots for reaction-diffusion systems*, J. Math. Biol., **57**(1), (2008), pp. 53–89.